U.S. DEPARTMENT OF THE INTERIOR
U.S. GEOLOGICAL SURVEY

THE COTTAGE LAKE AEROMAGNETIC LINEAMENT: A POSSIBLE ONSHORE EXTENSION OF THE SOUTHERN WHIDBEY ISLAND FAULT, WASHINGTON

By Richard J. Blakely[1], Brian L. Sherrod[2], Ray E. Wells[1], Craig S. Weaver[2], David H. McCormack[3], Kathy G. Troost[4], and Ralph A. Haugerud[2]

Open-File Report 2004-1204

2004

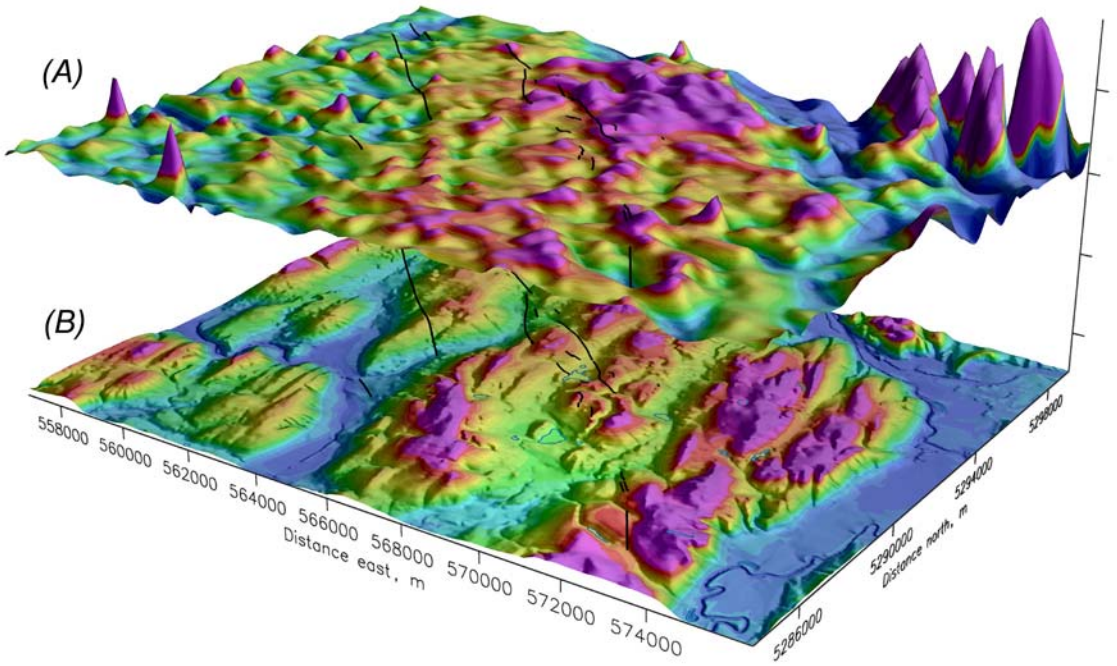

[1] U.S. Geological Survey, 345 Middlefield Road, Menlo Park, CA 94025
[2] U.S. Geological Survey, Box 351310, University of Washington, Seattle, WA 98195
[3] Aspect Consulting, 811 First Avenue, Suite 480, Seattle, WA 98104
[4] University of Washington, Department of Earth and Space Sciences, Box 351310, Seattle, WA 98195

Cover illustration: Three-dimensional view of aeromagnetic anomalies, terrain, and lidar scarps and lineaments. View is from southeast. (A) Residual magnetic anomalies. (B) Terrain from a 10-m digital elevation model, vertically exaggerated 2:1. Black lines are lidar scarps and lineaments discussed in text.

Copies of this USGS Open-File Report can be obtained at http://pubs.usgs.gov/of/2004/1204

CONTENTS

Figures

Tables

THE COTTAGE LAKE AEROMAGNETIC LINEAMENT: A POSSIBLE ONSHORE EXTENSION OF THE SOUTHERN WHIDBEY ISLAND FAULT, WASHINGTON

By Richard J. Blakely, Brian L. Sherrod, Ray E. Wells, Craig S. Weaver, David H. McCormack, Kathy G. Troost, and Ralph A. Haugerud

ABSTRACT

The northwest-striking southern Whidbey Island fault zone (SWIF) was mapped previously using borehole data and potential-field anomalies on Whidbey Island and marine seismic surveys beneath surrounding waterways. Abrupt subsidence at a coastal marsh on south-central Whidbey Island suggests that the SWIF experienced a M_W 6.5 to 7.0 earthquake about 3000 years ago. Southeast of Whidbey Island, a hypothesized southeastward projection of the SWIF would make landfall between the cities of Seattle and Everett. As part of systematic, ongoing studies by the U.S. Geological Survey, University of Washington, and other earth science organizations to evaluate potentially active faults and other earth hazards throughout the Puget Lowland, we test this hypothesis using aeromagnetic, lidar, and borehole data.

Linear, northwest-striking magnetic anomalies traversing the mainland region project southeastward toward the communities of Woodinville and Maltby, Washington. All of these magnetic anomalies are low in amplitude and best illuminated in residual magnetic fields. The most prominent of the residual magnetic anomalies extends at least 16 km, lies approximately on strike with the SWIF on Whidbey Island, and passes near Crystal and Cottage Lakes, about 27 km southeast of downtown Everett. In places, this magnetic anomaly is associated with topographic lineaments, but spectral analysis indicates that the source of the anomaly extends to depths greater than 2 km and cannot be explained entirely by topographic effects. The Alderwood #1 oil exploration well located on strike with the Cottage Lake aeromagnetic lineament shows evidence of deformation over a total depth range of 3000 m; some beds within this interval exhibit intense fracturing and shearing, although deformation within the well can only be constrained as post-early Oligocene and pre-Pleistocene. Boreholes acquired as part of a wastewater tunnel project show evidence of soil disturbance at locations where some topographic and aeromagnetic lineaments cross the tunnel alignment. Some of the disturbance is likely tectonic in origin, although other explanations are possible. Some of the soil disturbance demonstrably predates the 15-13 ka Fraser glaciation of the Puget Lowland; other samples have inconclusive ages and may be younger. Subtle scarps in Pleistocene surfaces are visible on high-resolution lidar topography at a number of locations along the Cottage Lake aeromagnetic lineament. Collectively, the scarps are parallel to the trend of the aeromagnetic lineament and extend a total distance of 18 km. In the field, scarps exhibit 1 to 5 m of north-side-up offset. The scarps provide targets for future paleoseismic trenching studies to test the hypothesis that they have a tectonic origin.

INTRODUCTION

Oblique subduction of the Juan de Fuca plate beneath North America produces a residual northward migration of the Washington and Oregon forearc toward Canada. Plate tectonic models, geodetic measurements, and geologic arguments indicate that this northward migration causes north-south shortening of the Washington forearc at the rate of about 6 mm/year on average (for example, Wells and others, 1998; Miller et al., 2001; Hyndman et al., 2003). Much of this deformation is accommodated on regionally extensive crustal faults that cross the Puget Lowland, including the Olympia, Tacoma, Seattle, southern Whidbey Island, and Devils Mountain faults (Figure 1). A rapidly growing body of paleoseismic evidence is showing that all of these Puget Lowland faults slipped during Holocene earthquakes (for example, Bucknam and others, 1992; Johnson and others, 2001, 2003; Nelson and others, 2003; Sherrod and others, 2004; Kelsey and others, 2004).

The southern Whidbey Island fault zone (SWIF) is a mostly concealed, northwest-trending structure extending across southern Whidbey Island toward Vancouver Island (Figures 1 and 2). The SWIF was first recognized and mapped at a regional scale by Gower and others (1985) on the basis of gravity and aeromagnetic anomaly maps. Johnson and others (1996) analyzed seismic-reflection profiles in the waterways around Whidbey Island, exposures in sea cliffs, and nearby borehole data and concluded that, on Whidbey Island, the SWIF consists of three main strands with strike-slip and reverse displacements. The northern and southern strands exhibit north-side-up displacement, whereas the middle strand has south-side-up offset and was interpreted as a backthrust rooted into the southern strand. Johnson and others (1996) inferred Quaternary deformation on the SWIF and estimated, based on its length, that the SWIF is capable of a M_S>7 earthquake. Kelsey and others (2004) found differences in relative sea-level histories at two coastal marshes located on opposite sides of a newly mapped trace of the SWIF (Figure 2). They interpreted their results as evidence for 1-2 m of vertical, north-side-up displacement during a M_W 6.5 to 7.0 earthquake about 3000 years ago.

The SWIF is associated with a diffuse zone of crustal earthquake epicenters (Figure 3) extending from the Strait of Juan de Fuca to the southern end of Whidbey Island. Associating specific earthquakes with specific faults is problematic throughout the Puget Lowland, however, and the relationship of the SWIF to the regional tectonic framework is complex. For example, focal mechanisms derived from three M>3.5 earthquakes in the mid-crust beneath the SWIF indicate mostly dextral strike-slip offset on northwest-striking, steeply dipping planes (Johnson and others, 1996). On the other hand, recent paleoseismic investigations of the Utsalady Point fault on northern Whidbey Island (Figures 1 and 3) suggest left-lateral displacements during late Holocene earthquakes (Johnson and others, 2003).

Along with the Tacoma and Seattle faults, the location of the SWIF affects earthquake hazard calculations for central and southern Puget Sound. While the location of the SWIF is relatively well known on Whidbey Island and surrounding waterways, it is not known whether, where, or how far the fault extends to the southeast. Johnson and others (1996) concluded on the basis of marine seismic-reflection data that three strands of the SWIF make landfall between Mukilteo and Nora Beach (Figure 2), and they suggested on the basis of regional geophysical data and tectonic arguments that these strands continue southeastward an additional 30 km. The

geophysical expression of the SWIF is subdued along its entire length, however, especially on the mainland southeast of Whidbey Island. In this paper we use numerical analysis of high-resolution aeromagnetic data, new lidar topographic surveys, and available subsurface information to investigate the proposed southeastward extension of the SWIF.

AEROMAGNETIC ANOMALIES

The aeromagnetic survey

In 1997, the U.S. Geological Survey conducted a high-resolution aeromagnetic survey of the Puget Lowland south of the Canadian border (Figure 4; Blakely and others, 1999). The purpose of the aeromagnetic survey was to contribute to ongoing geophysical and geologic investigations of geologic hazards throughout the Puget Lowland—Willamette Valley urban corridor in western Washington and Oregon. The Puget Lowland aeromagnetic survey was flown at an altitude of 250 m above ground, or as low as permitted by safety considerations. Over the study area to be discussed subsequently, the average altitude above ground was 262 m. Flight lines were directed north-south and spaced 400 m apart over the Puget Lowland; east-west tie lines were flown 8 km apart to facilitate data compilation. A theoretical flight surface, based on a digital topographic model, was computed in advance of the survey, and real-time, differentially corrected Global Positioning System (GPS) navigation was used during flight to maintain that desired flight surface. Two ground-based magnetometers operated continuously during the survey in order to monitor and correct for time-varying magnetic fields. Total-field measurements were reduced to anomaly values by subtracting the International Geomagnetic Reference Field updated to the date of the survey. Original measurements were spaced very closely along each flight and tie line. To alleviate artifacts in gridded and processed maps caused by this directional over-sampling, the original database was winnowed by 90 percent, producing an average along-line sample interval of 180 m.

The airborne and ground-based magnetometers used in the Puget Lowland aeromagnetic survey had sensitivities of 0.005 nT and noise levels of 0.02 nT, but several factors would tend to decrease the overall precision of the aeromagnetic maps. These include navigational errors, diurnal and transient effects, and aircraft magnetic fields. The Puget Lowland survey was conducted using standards established by the U.S. Geological Survey, including positional accuracies estimated at less than 5 m, the use of specially designed aircraft, in-flight compensation of aircraft magnetic fields, and stringent requirements on maximum allowable diurnal and transient magnetic fields. Taking all of the sources of error into consideration, we estimate the overall precision of individual measurements to be 0.5 nT or better.

Given the distribution of flight and tie lines and along-line sample spacing, the aeromagnetic survey has Nyquist wavelengths of approximately 800 m in the east-west direction and 360 m in the north-south direction. We are unable to completely resolve individual magnetic anomalies smaller than these horizontal dimensions. At 262-m altitude, however, even sources as small as discrete points and located as shallow as the topographic surface would produce anomalies with horizontal dimensions of about 600 m. Larger (more realistic) or deeper sources would produce anomalies with broader dimensions, and thus we believe the aeromagnetic survey has done an adequate job of sampling anomalies caused by near surface sources.

Volcanic rocks are typically more magnetic than other lithologies and produce distinctive magnetic anomalies when exposed at the surface or when located at shallow depths. A complex variety of volcanic rocks of varying ages and origins underlie the Puget Lowland. For example, strong positive magnetic anomalies (bright red areas on Figure 4) occur over the eastern margin of the Olympic Mountains, where basaltic rocks of the Eocene Crescent Formation are exposed at the surface or lie at shallow depth. Distinctive anomalies also occur over pre-Tertiary ophiolites in the San Juan Islands and contribute to a series of magnetic anomalies that help delineate the Devils Mountain fault (Johnson and others, 2001). Characteristic short-wavelength, high-amplitude anomalies occur over volcanic rocks of the Cascade Range, notably those surrounding Mount Rainier in the southeastern corner of the Puget Lowland aeromagnetic map (Figure 4).

Magnetic anomalies are typically subdued over sedimentary basins of the Puget Lowland, but notable exceptions exist. A steeply dipping layer of basaltic conglomerate lying within the Miocene Blakely Harbor Formation produces the narrow, linear anomaly that crosses southern Bainbridge Island (Figure 4; Blakely and others, 2002).

Faults that juxtapose rocks of contrasting magnetic properties at shallow- and mid-crustal depths produce linear magnetic anomalies, and all of the known, regionally extensive faults of the Puget Lowland are reflected in high-resolution aeromagnetic data (Figure 4). Deformation on the Seattle fault, for example, has incorporated various magnetic lithologies into shallow parts of its hanging wall, and these rocks produce distinctive magnetic anomalies that permit detailed mapping of the hanging-wall geology. The narrow anomaly crossing southern Bainbridge Island (Figure 4), for example, marks a Holocene strand of the Seattle fault, as evidenced by close spatial association of the magnetic anomaly with fault scarps exposed in trench excavations (for example, Blakely and others, 2002; Nelson and others, 2003; Sherrod, 2002).

Regional magnetic anomalies of the SWIF

Regional geophysical surveys reveal the broad crustal structure of the SWIF beneath the Puget Sound. Seismic tomography and gravity anomalies (Brocher and others, 2001) image the SWIF as a linear, northwest-trending contact between low-velocity, low-density sediments of the Everett basin and high-velocity, high-density Crescent Formation that underlies the Kingston arch (Figure 1). Marine seismic-reflection surveys have imaged three strands of the SWIF in the waterways around southern Whidbey Island, and interpretations based on these data indicate vertical, north- and south-side-up displacements at least as recently as Quaternary time (Johnson and others, 1996).

The SWIF also appears as a regional-scale linear aeromagnetic anomaly (Figures 2 and 4), first recognized by Gower and others (1985). Although aeromagnetic anomalies clearly identify the SWIF, its expression is broader and more subdued than those associated with other faults in the Puget Lowland (for example, Blakely and others, 2002). West of Whidbey Island (Figure 2), linear magnetic anomalies are clearly aligned along mapped strands of the SWIF. Southeast of Useless Bay, however, magnetic anomalies are longer in wavelength, and associating anomalies with individual fault strands is problematic. To first order, the magnetic expression of the SWIF reflects vertical offsets of highly magnetic basaltic rocks of the Eocene Crescent Formation against younger, less magnetic sedimentary deposits that fill the Everett basin to the north. The

broad nature of the anomaly over Possession Sound (Figure 2) indicates that offsets of Crescent Formation are relatively deep in this region, greater than several kilometers, a fact confirmed by seismic-reflection data (Johnson and others, 1996). Over the mainland and at the scale of Figure 2, the magnetic expression along the hypothesized southeastward projection of the SWIF is obscured, particularly in the region between Lake Washington and Everett. This suggests that offsets in Crescent Formation, if they exist beneath the mainland, lie at even greater depths than beneath Whidbey Island and Possession Sound. On the other hand, we note a subtle northwest-trending grain to the aeromagnetic anomalies in this mainland region (Figure 2) that may originate from magnetic rocks stratigraphically higher than the Crescent Formation.

Possible magnetic sources beneath the mainland projection of the SWIF

Two high-amplitude magnetic anomalies are evident between Snohomish and Woodinville (Figure 5), along the hypothesized southeastward projection of the SWIF. A pronounced circular anomaly (label A, Figure 5) lies over Tertiary mafic volcanic rocks exposed at Devils Butte and Bald Hill south of the town of Snohomish (Yount and Gower, 1991; Minard, 1985). Johnson and others (1996) considered these rocks equivalent to Eocene volcanic rocks of Mount Persis (Tabor and others, 1993), correlative with Tukwila Formation exposed 30 to 40 km to the south. Based on magnetic susceptibility measurements at four sites on and around Bald Hill, induced magnetization of relatively fresh volcanic exposures had an average magnetization of 0.73 A/m (Table 1). These mafic volcanic rocks probably cause anomaly A.

A broader magnetic anomaly of similar amplitude overlies Crystal and Cottage Lakes (label B, Figure 5). Glacial deposits exposed at the ground surface in this area are not sufficiently magnetic to account for the high amplitude of this anomaly (Table 1), and the broad gradients around the margins of the anomaly suggest that it originates from several kilometers below the surface. Eocene Crescent Formation or Eocene volcanic rocks of Mount Persis probably cause anomaly B. The linear northeastern margin of anomaly B suggests steeply dipping bedrock or fault control.

Superimposed on these pronounced, broad, high-amplitude magnetic anomalies is a subtle pattern of short-wavelength, low-amplitude anomalies, best displayed by the shadows in Figure 5. Man-made structures cause some of these anomalies. The distinctive anomaly located about 3 km southeast of Mukilteo and immediately north of State Route 526 (label C, Figure 5), for example, lies over a major Boeing facility and is probably caused by associated infrastructure. Much of the other short-wavelength, “noisy” pattern between Mukilteo and Edmonds is probably caused by human development.

Other low-amplitude anomalies in Figure 5 are caused by near-surface geology. Of particular interest are anomalies that extend linearly for many kilometers. These linear anomalies cannot be explained by man-made structures and probably originate from magnetic variations in geologic materials. In particular, the northwest-trending, linear anomaly near Cottage and Crystal Lakes, evident as a shadow on Figure 5 (label D, black arrows), is not obviously associated with roads, power lines, or other human development.

Although vertical offsets of Crescent Formation or other highly magnetic volcanic rocks appear to be relatively deep beneath anomaly B, as discussed above, deep exploratory wells in the area

indicate that overlying sedimentary rocks may also contribute to magnetic anomalies. In particular, two wells are located in the immediate region where the SWIF is hypothesized to project onto the mainland (Figure 5). The Standard Oil Company of California Alderwood #1 well reached a total depth of 3353 m (Rau and Johnson, 1999). Drilling encountered unconsolidated Pleistocene glacial and interglacial deposits to depths of 110 m, then penetrated mudstone, siltstone, and sandstone of the upper Eocene to lower Oligocene Blakeley Formation to a depth of 1591 m.

Glacial deposits and Blakeley Formation are generally considered nonmagnetic (for example, Finn, 1990; Blakely and others, 2002). However, sandstone and siltstone observed within the Blakeley Formation of the Alderwood #1 well were commonly tuffaceous (Rau and Johnson, 1999) and thus may be weakly magnetic. Moreover, minor correlations between glacial topography and magnetic anomalies, noted subsequently, suggest that glacial deposits also might be slightly magnetic. In an attempt to verify this, we made a number of magnetic susceptibility measurements in the Woodinville-Maltby area, summarized in Table 1. We visited five locations of Vashon-age recessional outwash and older Pleistocene glacial deposits and found average induced magnetizations ranging from 0.05 to 0.12 A/m, with an overall average value of 0.09 A/m. We also conducted magnetic susceptibility measurements of four bedrock exposures in the Maltby area mapped as upper Eocene to lower Oligocene Blakeley Formation (Minard, 1985). Fine-grained exposures had an average induced magnetization of only 0.01 A/m, but one pebbly bed had an average magnetization of 0.11 A/m. These weak values are sufficient to produce low-amplitude magnetic anomalies at low aircraft altitudes, as demonstrated subsequently.

Between depths of 1591-3353 m, the Alderwood #1 well passed through sedimentary and volcanic rocks interpreted by Rau and Johnson (1999) as Eocene sandstone of Scow Bay. Within this interval, eight or more intervals of volcanic rock and volcanic conglomerate had thicknesses up to 46 m. Based on five samples from the well, 80 percent of the volcanic rock had basaltic composition; the remainder was andesitic in composition (Rau and Johnson, 1999). Offsets of these volcanic units within the Eocene sandstone of Scow Bay also could produce subtle magnetic anomalies.

The Standard Oil Company of California Socal-Schroeder #1 well (Figure 5; Rau and Johnson, 1999) passed through 207 m of unconsolidated Pleistocene glacial and interglacial deposits, then penetrated Blakeley Formation and Renton Formation to a depth of 2438 m. From 2438 to 2697 m, drilling penetrated andesitic volcanic rocks interbedded with carbonaceous mudstone and siltstone, interpreted by Rau and Johnson (1999) as upper Eocene volcanic rocks of Mount Persis (Tabor and others, 1993). Similar rocks are exposed at Devils Butte and Bald Hill, where they produce a high amplitude magnetic anomaly (label A, Figure 5) and have moderate values of magnetic susceptibility (Table 1). These buried volcanic deposits could produce low-amplitude magnetic anomalies at aircraft altitudes.

Analysis of aeromagnetic data

Numerical processing of aeromagnetic surveys often reveals subtle trends related to important structures not readily seen in the regional-scale analysis (for example, Ponce and others, 2003; Grauch and others, 2001). Three numerical methods were applied to the Puget Lowland aeromagnetic survey in an attempt to emphasize subtle, linear anomalies presumably caused by shallow geologic sources. These methods are described in the following subsections and in Figures 6 through 11.

Residual magnetic anomalies

The first method capitalizes on the fact that the intensity of a magnetic field decreases with distance from the object that causes the magnetic field. The field intensity over a spherical magnetic source, for example, is proportional to $1/r^3$, where r is the distance between the magnetic sensor and the center of the sphere (Telford and others, 1990; Blakely, 1995). Suppose we have two aeromagnetic surveys over the same distribution of magnetic sources, the only difference being the altitudes of the surveys above ground. Each magnetic anomaly in the upper survey will have lower amplitude than its counterpart in the lower survey, but, because of the $1/r^3$ rule, the amount of that attenuation will depend on the depth of each respective source: deeper sources will be less attenuated than shallow sources. Given only a single aeromagnetic survey, we can exploit these characteristics with a two-step procedure: We first analytically continue the aeromagnetic survey upward a small distance, then subtract that result from the original survey. This procedure tends to accentuate anomalies due to shallow magnetic sources at the expense of those caused by deeper sources. This method is essentially a discrete vertical derivative of the magnetic field, well known as a way to accentuate shallow magnetic sources (Telford and others, 1990; Blakely, 1995).

Figure 6 demonstrates these principles with a hypothetical example using actual data. The map on the left (Figure 6A) shows actual measured aeromagnetic anomalies. To simulate a near-surface fault in weakly magnetic sediments a very low-amplitude magnetic anomaly has been artificially added to these data. It is difficult if not impossible to detect the anomaly caused by the hypothetical fault in the original data (Figure 6A). The map on the right (Figure 6B) shows the same data after application of the residual method. Large-amplitude anomalies due to deep sources are now greatly subdued, and the linear anomaly caused by the hypothetical fault is more evident.

Figure 7 shows the residual method applied to aeromagnetic data over the study area. Magnetic anomalies caused by deep sources are still prominent but significantly reduced in amplitude relative to the original data (Figure 5). This procedure naturally amplifies the magnetic signal of manmade structures at the topographic surface. For example, large buildings, like hospitals and skyscrapers, often produce distinctive, more or less symmetric anomalies that are easily recognized. The most obvious example in Figure 7 is the complex, roughly circular anomaly 3 km southeast of Mukilteo. It has peak-to-trough amplitudes in Figure 7 of approximately 190 nT, is located over a major Boeing facility, and is probably related to manmade structures. Linear anomalies sometimes coincide with major freeways because freeways incorporate

metallic building materials. However, we see no evidence in Figure 7 that linear anomalies are associated with freeways or major highways.

Many linear anomalies evident in Figure 7 are not associated with manmade objects and must have geologic explanations. In particular, a northwest-striking gradient passing near Crystal and Cottage Lakes is continuous over a length >16 km and not associated with manmade objects. Other northwest-striking anomalies in Figure 7 have similar expression. These anomalies are very low in amplitude, with peak-to-trough amplitudes generally less than 8 nT. We focus here on the Cottage Lake aeromagnetic lineament (label D, Figure 7) for reasons described in the following section.

Magnetic boundary analysis

The second method emphasizes contacts between magnetic and less magnetic rocks. It capitalizes on a mathematical connection between magnetic anomalies and gravity anomalies: Given only the magnetic anomaly measured over a distribution of magnetic sources, it is possible to calculate the gravity anomaly expected over an identical distribution of gravity sources (Baranov, 1957; Telford and others, 1990; Blakely, 1995). This transformation, known as *pseudogravity*, requires no assumptions regarding the true nature of the magnetic sources, other than the vector orientation of magnetization. The pseudogravity transformation is of interest in our application because gravity anomalies are in some ways easier to interpret than magnetic anomalies. For example, a gravity anomaly over a tabular mass has maximum horizontal gradients located over the edges of the mass, whereas the dipolar nature of magnetic sources produces magnetic anomalies with highs and lows, a shape that depends on both the direction of magnetization and direction of the ambient field (Figure 8). We extend this advantageous characteristic of gravity anomalies to analysis of aeromagnetic anomalies with a three-step procedure (Blakely and Simpson, 1986): (1) We transform magnetic anomalies to pseudogravity anomalies, (2) calculate the maximum horizontal gradient at each point, and (3) plot the location of each maximum. Figure 9 shows this method applied to the aeromagnetic data over the study area, where alignments of white dots indicate abrupt contrasts in magnetization. This method has the important advantage of providing an objective interpretation, not influenced by pre-determined geologic models. No assumptions about the magnetic source are required except an assumed knowledge of the vector direction of magnetization, which we here assume to be parallel to the ambient field of the earth.

These aeromagnetic lineaments have various geologic explanations (discussed below), but those that trend northwestward are most relevant for testing the hypothesis of possible onshore projections of the SWIF. Figure 10 identifies significant northwest-striking magnetic lineaments. Black dashed lines on Figure 10 indicate interpreted lineaments associated with specific magnetic boundaries (white dots of Figure 9), as determined numerically with the method of Blakely and Simpson (1986). Black dotted lines are interpreted lineaments with lower confidence, drawn on the basis of alignment, offset, or truncation of individual anomalies. Using continuity of white dots (Figure 9) as a measure, the Cottage Lake aeromagnetic lineament is the longest, most continuous northwest-striking magnetic gradient of the study area. Even still, the Cottage Lake aeromagnetic lineament is much lower in amplitude relative to magnetic anomalies along mapped traces of the SWIF west of Whidbey Island (Figure 2).

Matched-filter analysis

The third method (Figure 11) exploits the fact that the *shape* of a magnetic anomaly depends on the depth to its magnetic source. For example, a deep source will produce a broader, smoother anomaly relative to the same source located at shallower depths. These wavelength characteristics are best described in the Fourier domain as power-density spectra, where the power of a deep-source anomaly falls off more rapidly with increasing wavenumber than the power of a shallow-source anomaly (Spector and Grant, 1970; Blakely, 1995). In principle, the shape of a power-density spectrum of a magnetic anomaly caused by a stack of magnetic layers can be analyzed to estimate the layer depths (Spector and Grant, 1970). Once determined, matched filters are designed to emphasize anomalies originating from important individual layers (Syberg, 1972; Phillips, 1997). In applying the matched-filter technique to the data of Figure 5, we determined four important layers at depths of 107, 433, 1245, and 2723 m. Table 2 shows our interpretation of each of these layers, and Figure 11 shows magnetic anomalies filtered to emphasize sources within a layer with top at 1245 m depth. We interpret this map as a reflection of offset of or lateral variations within magnetic lithologies between 1 and 2.5 km below the topographic surface. Existing borehole control suggests that the source layers may include volcanic rocks or volcanic conglomerate within the Tertiary sandstone of Scow Bay or Tertiary volcanic rocks of Mount Persis (Rau and Johnson, 1999). Most of the northwest-striking lineaments interpreted from previous maps are evident in this filtered version (interpreted black dashed and dotted lines, Figure 11), indicating that these northwest-striking sources extend to depths greater than 2 km.

Consideration of possible artifacts

Each of the above methods involves Fourier-domain calculations, and thus we should consider the possibility that northwest-trending features seen in the processed data are artifacts due to edge effects, aliasing, or other computational errors. Edge-effect artifacts, as the name implies, tend to be near and oriented parallel to the edges of the gridded database. If they exist at all in our results, they do not cause the northwest-trending anomalies described above. We also do not regard aliasing or uneven sample distribution to be serious problems, for the reasons discussed above. Moreover, anomaly D and other northwest-trending magnetic lineaments appear in the original aeromagnetic data (Figure 5); their presence in the derivative maps (Figures 7 and 9-11) cannot be the result of processing artifacts.

In summary, high-resolution aeromagnetic measurements over the study area indicate a subtle pattern of northwest-striking anomalies best displayed in processed versions of the original magnetic data. Geologic interpretation of those anomalies is discussed below.

Geologic interpretation of magnetic anomalies

Northwest-striking magnetic anomalies in Figures 5, 7, and 9-11 are interpreted as originating from alignments of weakly magnetic sedimentary rocks and thin interbedded volcanic layers in the upper few kilometers of the earth's crust. Later we will describe spatial correlations between some of these anomalies and lidar topography and regional digital elevation models. Various geologic explanations for these anomalies should be considered (Figure 12).

In some situations, shallow materials underlying the terrain itself may be magnetic and thus produce magnetic anomalies that correlate with topography (Figure 12B). Under ideal conditions, the pilot flying the aeromagnetic survey strives to maintain constant altitude above all topographic features. In practice, fixed-wing aircraft never completely achieve this goal, flying near the ground over ridge tops and farther from the ground over valleys, and variable clearance above weakly magnetic terrain can produce low-amplitude anomalies. Weakly magnetic sediments forming the sea cliffs probably cause the anomalies along coastlines in Figure 5, for example, particularly along the southern coast of Whidbey Island and the west coast of the mainland. Later in this report we contrast the relative anomaly amplitudes that might originate from terrain verses from deeper layers. In any case, it is unlikely that the northwest-striking gradients in the study area can be explained entirely in this way because few if any of these lineaments correlate with variations in terrain clearance (Figure 13B). Exceptions occur over the Snohomish and Skykomish Rivers, where the rivers wrap around the steep slopes of Devils Butte and Bald Hill, and over the Sammamish River, where it empties into Lake Washington. We note that the anomaly near Crystal and Cottage Lakes (label D, Figures 5, 7, 9-11), the longest of the northwest-striking anomalies, shows negligible correlation with variations in aircraft altitude above ground.

The growth of secondary magnetic minerals along concealed fractures or faults could produce linear magnetic anomalies in the study area (Figure 12C). Such processes occur in some geologic environments. Linear magnetic anomalies in northern Nevada, for example, reflect epithermal processes related to large distal volcanic systems, where secondary magnetic minerals have been concentrated in pre-existing fracture zones (Ponce and Glen, 2002). Although much smaller in size, the volcanic rocks that underlie Devils Butte and Bald Hill are described as partially intrusive (Minard, 1985), and a Tertiary pluton may have provided a possible source for secondary mineralization. We cannot rule out the possibility that such processes occurred in our study area, but existing geologic mapping shows no evidence of such concentrations.

The most likely explanation for the northwest-striking anomalies is simply the juxtaposition of lithologies having slightly contrasting magnetic properties. These contacts may be due to crustal faulting (Figure 12D) or to depositional processes (Figure 12E) now concealed by younger glacial deposits. In the first case, correlations between magnetic anomalies and topographic lineaments and scarps may reflect tectonic deformation of the topographic surface; in the latter case, correlations between magnetic anomalies and topographic lineaments and scarps may reflect lateral variations in resistance to erosion that correspond to variations in magnetic properties. Pronounced linear contacts extending over many kilometers are commonly due to faulting or folding. We cannot determine the age of the fault from aeromagnetic data alone. An older, inactive fault scarp could cause the anomalies.

SUBSURFACE INFORMATION

The Standard Oil Company of California Alderwood #1 well is located within the hypothesized onshore projection of the SWIF (Figure 14) and on strike with the Cottage Lake aeromagnetic lineament. Oil company descriptions of the Alderwood #1 well (Standard Oil Company of California internal document, 1947) document evidence of tectonic deformation between depths of 1209 and 2713 m, variously described as slickensides, fault gouge, and “badly crushed” or

"badly fractured" strata. Rau and Johnson (1999) reexamined the Alderwood #1 well and also found evidence of subsurface deformation. Strata within the Oligocene Blakeley Formation (depths from 268 to 1591 m) were commonly fractured and sheared, and beds within the deeper sandstone of Scow Bay (depths from 1591 to 3353) were intensely sheared (Rau and Johnson, 1999). No deformation was noted in strata younger than the Blakeley Formation, about 35 Ma. Thus the age of deformation in the Alderwood #1 well is only constrained to be post-early Oligocene and pre-Pleistocene. Rau and Johnson (1999) noted no deformation in the Socal-Schroeder #1 well.

Subsurface explorations are underway to support design and construction of 30-km of wastewater conveyance tunnels between the Woodinville area and a marine outfall in Puget Sound south of Edmonds, Washington (Figure 14). Explorations consisting of 157 boreholes to an average depth of 75 m have been completed along the conveyance alignment (CDM, 2004), allowing a detailed geologic profile to be constructed across much of the study area. Conveyance borehole core samples are being analyzed for evidence of subsurface disturbances, such as shearing, slickensides, fracturing, brecciation, low soil strength, and other indications of post-depositional stress.

Soil disturbance was encountered in many boreholes throughout the conveyance alignment. The locations of boreholes exhibiting at least one vertical zone of continuous disturbance are presented on Figure 14. Although some of the sample disturbance is likely tectonic in origin, soil disturbance of this type can also result from modern or ancient landslides, ice loading or ice contact, soft sediment loading and fluid escape, liquefaction, and bioturbation, The drilling and sampling process can also induce disturbance. Some of the disturbed structures are tightly rehealed, indicating that they have been glacially overridden and that the disturbance predates the 15-13 ka Fraser glaciation of the Puget Lowland. In other samples, the disturbance appears to be younger. However, since drill or sample-induced disturbance may account for some or all of the apparently younger disturbance, it is not possible to conclusively determine the relative age or cause of this apparently post-Fraser sample deformation. Ongoing design studies are likely to provide additional soil and geologic data beneficial for subsurface evaluation.

The pattern of disturbance does not directly correlate with interpreted magnetic or topographic lineaments. Two boreholes exhibiting soil disturbance are located beneath a northwest-striking aeromagnetic lineament (label E, Figure 14) that passes about 1 km southwest of Woodinville, and other disturbed boreholes are on strike with several aeromagnetic lineaments (labels F, G, and H, Figure 14) extending southeast from Edmonds. On the other hand, other aeromagnetic lineaments identified on Figure 14 (label I and J) show no relation to soil disturbance. The Cottage Lake aeromagnetic lineament (label D, Figure 5, 7, 9-11) does not cross the conveyance project, and it will not be possible to correlate between sample disturbance and this hypothesized projection of the SWIF.

LIDAR GEOMORPHOLOGY

Lidar (light detection and ranging, also known as ALSM, airborne laser swath mapping) is an airborne technique to determine topographic elevations with high precision (Haugerud and others, 2003). Using a narrow laser beam to penetrate through tree cover, lidar surveys can produce accurate terrain maps even where forest cover largely obscures the ground surface. In

the highly vegetated Puget Lowland, lidar has proved a boon in discovering previously unrecognized scarps and other geomorphology (Haugerud and others, 2003).

In this report, we define a *scarp* as a line of cliffs or topographic steps produced by faulting or erosion (Bates and Jackson, 1980). A *fault scarp*, on the other hand, refers to a line of cliffs or steps caused by surface rupture during an earthquake. *Possible scarps* are features that resemble scarps in the lidar data, but lidar profiles, local geomorphology, or field observations do not clearly confirm their existence. A *topographic lineament* is defined as a linear alignment of landforms, including streams, low ridges, steps, cliffs, and ravines, and may be the result of faulting, erosion, or glacial processes. Because none of the features identified in this report have been studied in detail, we cannot attribute any scarp to an earthquake or faulting event, nor can we preclude the possibility that faulting was responsible for such scarps. Detailed field work is required before any *scarp* can be categorized as a *fault scarp*. In some cases, however, the geomorphology of the feature and surrounding area suggest a particular origin for a scarp (landslides, for example). Our work so far has been aimed at identifying *possible* tectonic features, some of which will be the focus of future detailed field studies.

Lidar data provided by King County and the Puget Sound Lidar Consortium were used in a GIS analysis to look for scarps and other topographic evidence of fault locations. We focused our search on the Woodinville-Maltby area for four reasons: First lidar data are not available throughout the study area (Figure 15B). In particular, the region west of SR 99 and much of the northeastern portion of the study area are not yet surveyed. Second, the Woodinville-Maltby area lies on strike with the hypothesized southeastward projection of the SWIF, and our primary objective was to evaluate the potential southeastward extension of this structure. Third, the Cottage Lake aeromagnetic lineament, the principal magnetic lineation identified within our study area and the most likely candidate for a subsurface fault, trends through the Woodinville-Maltby area. Recent studies elsewhere have noted the close association of aeromagnetic anomalies and fault scarps (for example, Sherrod, 2002; Sherrod and others, 2004; Nelson and others, 2003; Blakely and others, 2002). Fourth, the region west of the Woodinville-Maltby area is highly urbanized (crosshatch pattern, Figure 5). Lidar data throughout much of this area are not useful for identifying possible scarps because of extensive ground surface alteration for human development. In any case, our interpretations throughout the study area should be considered preliminary.

Our analysis primarily used visual examination of hillshaded relief images, simultaneously illuminated from azimuths of 315°, 0°, and 45°, at a sun angle of 45°, and with no vertical exaggeration. Our purpose was to map the population of scarps and topographic lineaments along the hypothesized SWIF. The grayscale topographic relief images were also draped with a semitransparent grid of residual magnetic anomalies to facilitate comparison with aeromagnetic data (Figure 15A). The resulting images show which of the scarps and topographic lineaments are associated with linear aeromagnetic anomalies having a crustal source.

Features identified from lidar data

Images calculated from high-resolution lidar data from the Cottage Lake area (Figures 15A) show several features important in understanding the geological history of the area. The images show linear glacial flutes that indicate flow directions of the last ice sheet, which flowed across this region about 16 ka (Porter and Swanson, 1998), and more subtle features, such as scarps and lineaments that cut across the glacial flutes at various locations. The following sections describe the topographic features observed in the lidar images and in the field. The text uses geographic names found on USGS 7.5' topographic maps to guide the reader in locating features on topographic and street maps. We first present a short description of processing artifacts in the lidar data, followed by a description of glacial flutes and ice flow directions in the study area, and end with a description of each scarp and topographic lineament.

Processing artifacts in the lidar data

Several processing artifacts are seen throughout the lidar data obtained from King County, specifically "pyrite forests" and swath boundary offsets. Descriptions of several common lidar artifacts, including pyrite forests, are located at the Puget Sound Lidar Consortium website: http://duff.geology.washington.edu/data/raster/lidar/lidardata/index.html.

Swath boundary offsets are sinusoidal features that, in these data, trend east-west. The lidar data were collected as narrow, east-west trending strips, or swaths, and then pieced together (see URL above for a short discussion of lidar processing by David Harding, a NASA lidar specialist). If, as is common, one swath of data is slightly tilted relative to the neighboring swath, the pieced-together surface will have a vertical step at the boundary between swaths. Steps smaller than about 15 cm (6 inches) may not be visible in images calculated from the lidar data. In data examined here, however, the steps are locally as large as 0.6 m (2 feet). The swath boundaries are sinusoidal because of roll of the aircraft that carried the lidar instrument. We identified and marked these artifacts whenever noted in order to avoid interpreting them as landforms. Our evaluations were conservative; if a lineament might have been a processing artifact, it was not considered further.

Glacial flutes

Glacial flutes are linear topographic features created by flowing ice and subglacial meltwater. Maps showing former ice flow directions are created by drawing lines along the crests of these flutes and along the bottoms of the interfluves (Figure 15A). Two ice-flow trends are observed in the study area: (1) roughly north to south (azimuth of ~175°) in the western part of the study area, and 2) slightly southeast (azimuth of ~165° to ~160°) in the eastern part of the study area. These former ice flow directions are important for our study because topographic features that cut across the flutes at high angles are likely not related to glaciers and probably reflect post-glacial processes.

Scarps and topographic lineaments

We identified 21 possible post-glacial features in our preliminary examination of the lidar images and grouped them as scarps, possible scarps and topographic lineaments (Figure 15A, Table 3). Azimuths of individual features range from about 120° to 145° and thus at an oblique angle to the glacial flutes described above. The 21 features are described below, progressing generally from the northwest to the southeast. Numbers at the beginning of each description are keyed to Figure 15A.

1. Lineament 1 trends northwest-southeast for approximately 2 km along several aligned stream channels and small ridges (Figure 16). The topographic lineament cuts across North Creek and sub-parallel to and about 2 km south of the Cottage Lake aeromagnetic lineament (Figure 14).

2. Lineament 2 trends northwest-southeast for about 7.5 km along several aligned streams and low, linear ridges (Figure 16). The lineament begins about a kilometer southeast of Martha's Lake, crosses North Creek near Thrasher's Corner, and ends at SR 522. Lineament 2 is adjacent to an aeromagnetic anomaly at its southeastern end (Figure 14).

3. Lineament 3 follows linear ridges and aligned stream channels for 2.25 km (Figure 16). The lineament begins about 1.5 km northeast of Kennard Corner and trends southeast before terminating several hundred meters east of Bear Creek. This topographic lineament lies on or near and is parallel to the Cottage Lake aeromagnetic lineament.

4. Lineament 4 is about 3 km long and follows the lower Bear Creek drainage (Figure 17). The lineament crosses SR522 about 1 km northeast of the intersection of SR 522 and SR 9. The southeastern part of the lineament is aligned along a deep ravine, a low ridge or scarp, and two additional scarps (see #8 below). The topographic lineament lies parallel to and along an aeromagnetic anomaly about 1.5 km southwest of the Cottage Lake aeromagnetic lineament.

5. Lineament 5 is a short alignment (~750 m long) of low ridges or scarps at Turner's Corner (intersection of SR 9 and 212th St. SE). A series of parallel linear ridges are seen in the lidar data at this location, the most prominent of which is marked on Figure 17. These features appear on the landscape between two aeromagnetic anomalies - the Cottage Lake aeromagnetic lineament and an aeromagnetic anomaly about 1.5 km to the southwest (Figure 14). Field observations in this area confirmed the presence of low linear ridges along lineament 5.

6. Feature 6 is a short, low scarp (Figures 17 and 18) along the Cottage Lake aeromagnetic lineament. The scarp trends northwest-southeast and is roughly aligned with the northwest end of lineament 7 (see below). A profile across the scarp (using the lidar data) shows that the scarp is north-side-up and has a maximum height of about 2 m (Figure 18).

7. Lineament 7 is a topographic alignment about 2.5 km long consisting of aligned streams, ravines, and low ridges (Figure 15A, 19). The topographic lineament begins near Turner's Corner at the southeast end of feature 6 and ends at the north end of Crystal Lake. The lineament lies along the Cottage Lake aeromagnetic lineament.

8. Two short scarps (~250 m) along the southeast end of lineament 4 show field evidence for north-side-up deformation (Figures 15 and 17). Profiles extracted from the lidar data across these scarps show two sub-parallel, north-side-up scarps, each about 2 m high (Figure 20). We believe that these scarps may be related to landslide deformation: Discussions with the owner of property located at the northwest end of these scarps suggest small amounts of on-going mass wasting; for example, about one inch of displacement on a sewer line and small cracks in a garage floor were noted after the 2001 Nisqually earthquake.

9. Feature 9 consists of two small scarps near the northwest shoreline of Crystal Lake (Figures 15A and 21). The scarps are between 750-1000 m long, are roughly perpendicular to the shoreline of Crystal Lake, and trend sub-parallel to the Cottage Lake aeromagnetic anomaly (Figure 14). These scarps are associated with a small swale in the road along the west shoreline of Crystal Lake. Lidar images of these scarps suggest the north sides are approximately 2 m higher than the south sides.

10. Feature 10 is the most prominent scarp observed in the lidar data (Figures 15A and 22). The scarp is about 1.5 km long, is sub-parallel to the eastern shoreline of Crystal Lake, and lies along the Cottage Lake aeromagnetic lineament (Figures 14 and 15A). Scarp 10 is aligned with lineament 7 to the northwest and joins with lineament 11 to the southeast, continuing southeast along the Cottage Lake aeromagnetic lineament for another 1.5 km. Lidar profiles across feature 10 (A-A' and B-B', Figure 22) show a broad, north-side-up scarp between 2.5 and 4 m in height. Field observations confirmed the scarp location and approximate height. The scarp is not clear on the lidar map at its southeast end due to poor lidar returns in dense vegetation.

11. Lineament 11 consists of a low, north-side-up ridge or scarp (Figures 15 and 23). This feature begins at the southeast end of feature 10 and continues to the southeast along the Cottage Lake aeromagnetic lineament for 1.5 km. A lidar profile across the feature (C-C', Figure 23) shows a broad, north-side-up scarp at least 4 m high. Field observations confirm the presence of a scarp in places, but dense vegetation made it difficult to trace the feature in the field. At other field locations, feature 11 resembles a small swale.

12. Feature 12 is a short, arcuate scarp located about 750 m northeast of feature 10 (Figures 15A and 23). Additionally, two faint arcuate features observed in the lidar data are located between features 12 and 10 (not marked on map because the features were so faint in the data). A profile across this feature (D-D', Figure 23) using the lidar data shows a 4 m high, north-side-up scarp. The size and shape of this feature suggest a landslide origin.

13. Feature 13 is a short, straight scarp located about 1 km east of feature 12, at the top of the bluff (about 200 m west of Paradise Lake Rd.) along the west side of Paradise Valley (Figures 15A and 24). Scarp 13 is ~100-200 m long and trends northwest-southeast, approximately parallel to the bluff edge (Figure 24). This feature is probably not a landslide: The hillshaded lidar map shows that this scarp has north side up, whereas a landslide at this location would produce a northeast-facing headscarp. Scarp 13 is 1.2 km northeast of the Cottage Lake aeromagnetic lineament. No field observations are available for this feature.

14. Lineament 14 is an alignment of ravines and a low ridge on the west side of Crystal Lake (Figure 25). The lineament is roughly parallel to the Cottage Lake aeromagnetic lineament and

is on strike with feature 15, a small scarp located at the south end of Crystal Lake. A lidar profile (Figure 25) indicates north side up. No field observations are available for this feature.

15. Feature 15 is a small scarp located at the south end of Crystal Lake (Figure 15A). The scarp is about 500 m long and trends northwest-southeast across a formerly clear-cut area (Figure 26). A profile across the scarp using the lidar data shows that the north-side-up scarp sits on a surface sloping gently to the northeast. The scarp is 3 m high at the location where the lidar profile was drawn – poor lidar returns in most of this area prevented further assessment of scarp heights. However, field observations of the scarp are consistent with the height and aspect shown in Figure 26.

16. Feature 16 consists of three short, en-echelon scarps that lie about 1 km southwest of the Cottage Lake aeromagnetic lineament (Figures 15A and 27). Detailed lidar images show individual scarps 150-200 m long with north side up (Figure 27). A profile across the southernmost scarp of feature 16 shows a low (~2 m high), broad (~20 m wide) scarp (Profile A-A' on Figure 27).

17. Feature 17 is a 500-m-long scarp located about 300 m east of the southern end of feature 16 (Figure 15A and 27). The scarp cuts through a developed area and is likely somewhat modified by landscaping and construction. The scarp cuts across a small ravine at its northern end. A profile across the middle of feature 17 shows a 5-m-tall, north-side-up scarp (Profile B-B' on Figure 27).

18. Feature 18 is a series of en-echelon and parallel scarps located about 2.5 km southeast of the intersection of Mink Rd. NE and NE Woodinville-Duvall Rd. (Figure 28). The scarps are sub-parallel to a prominent magnetic anomaly along the southern end of the Cottage Lake aeromagnetic lineament (Figure 15A). The most prominent scarp is about 2 km long (Figure 28). Lidar profiles across this scarp show broad (>15 m in places), north-side-up topography reaching maximum heights of 2 to 3 m (Figure 26). Field observations confirm the presence of a broad scarp consistent with the lidar image of feature 18. The scarp cuts through a developed area and is likely modified from its original morphology in places.

19. Lineament 19 consists of an alignment of streams and low ridges at the south end of the Cottage Lake aeromagnetic lineament (Figure 15A). The lineament trends north-northwest sub-parallel to nearby glacial flutes.

20. Lineament 20 consists of an alignment of low ridges or scarps northeast of the intersection of 210th Avenue NE and Novelty Hill Road in Redmond, Washington (Figure 15A). These short features appear as low (~1 m), en-echelon scarps and trend sub-parallel to nearby glacial flutes.

21. Feature 21 is a broad north-side-up scarp located at the junction of valleys occupied by Bear Creek and the Sammamish River (south of the intersection of SR 522 and SR 202 in Woodinville; Figure 15A). The scarp is broad in comparison to other scarps observed in lidar data and is parallel to the Sammamish River (roughly NW-SE). The geomorphology of the surrounding area suggests that the scarp likely represents a riser (vertical, steeply sloping step) between two fluvial terraces – one in the Bear Creek valley and the other in the Sammamish River valley.

Features considered for further field study

Our analysis of lidar images and field observations lead us to conclude that scarps 10, 11, 15, and 18 are the most likely candidates for further field study. This conclusion is based on their proximity to the Cottage Lake aeromagnetic lineament, distinctness of the lidar trace, characteristics of the lidar profiles, and field observations that, among other factors, demonstrate the feasibility of trenching across them. Trenching across scarps could help determine their origin and could yield information on the presence or absence of past earthquakes on the hypothesized projection of the SWIF.

DISCUSSION

In summary, we have found evidence for very low-amplitude, northwest-trending magnetic anomalies between Snohomish and Lake Washington (Figures 5, 7, 9-11), which are on strike with a hypothesized southeastward projection of the SWIF. The longest of these anomalies lies near Crystal and Cottage Lake and extends continuously for about 18 km. The Cottage Lake aeromagnetic anomaly is on strike with the Alderwood #1 well (Figure 14), where Oligocene and older sedimentary rocks are deformed. Boreholes in the area between Woodinville and Puget Sound show evidence of Pleistocene soil disruption consistent with tectonic disturbance, although other explanations are possible. Some of the borehole disturbance is demonstrably older than Fraser glaciation (15-13 ka), whereas the age of other disturbances are inconclusive. The association of disturbed boreholes with specific aeromagnetic lineaments is problematic. We also have examined lidar data from the Woodinville-Maltby area and found evidence of 21 topographic scarps and lineaments (Figure 15A). The most prominent scarps are located near Crystal and Cottage Lakes where, considered together, the scarps and associated topographic lineaments extend for about 18 km, are coincident with and sub-parallel to the Cottage Lake aeromagnetic lineament (Figure 14), and are sub-parallel to the hypothesized southeastward projection of the SWIF from Whidbey Island. In the field, the scarps are typically 2 to 3 m high (maximum of 5 m), north side up, and cut the latest Pleistocene glaciated surface. In comparison to other lidar scarps of the Puget Lowland (for example, Nelson and others, 2003), the Crystal and Cottage Lake scarps are subtle features, but their close spatial association with the Cottage Lake aeromagnetic lineament is suggestive of a common origin.

In addition to spatial association with 2-5-m high scarps, the Cottage Lake aeromagnetic lineament (label D, Figure 5, 7, 9-11) also correlates with larger topographic features observed on topographic quadrangle maps and digital elevation models. Figure 13A shows the interpreted northwest-striking aeromagnetic lineaments plotted on a topographic map derived from a 10-m digital elevation model. North of Cottage Lake, the Cottage Lake aeromagnetic lineament swings northward to follow the Cottage Lake Creek drainage for approximately 2 km. The lineament also passes through a gap between two offset glacial ridges located about 2 km north-northwest of Crystal Lake, and similar correlations are seen elsewhere along this and other aeromagnetic lineaments.

A variety of large-scale linear topographic features are apparent in the modern landscape. The mostly north-south troughs of Puget Sound are the result of subglacial drainage (Booth and Hallet, 1993); the roughly north-south elongated ridges and valleys in the Puget Lowland are

glacial drumlins and interdrumlin valleys resulting from glacial processes (Goldstein, 1994; Booth et al., 2003). A number of small to large channels, some with modern streams and some without, crosscut this overall north-south grain. Most of these are glacial recessional channels related to varying ice retreat positions. Included in this group are many northwest-trending valleys across the Puget Lowland such as McAleer Creek, the Seattle ship canal valley, the Duwamish valley, and the downstream end of the Puyallup valley. The reasons for the locations of these valleys are not always obvious. They could simply have been shallow post-glacial or subglacial troughs, later exploited and expanded by recessional meltwater. Some do coincide with aeromagnetic anomalies, but most do not. A tectonic origin is inadequate to explain them all. Of the most prominent of the northwest-trending valley lineations, the Seattle ship canal does not correspond to any known tectonic anomaly, whereas the lower Puyallup valley does correspond to a possible strand of the Tacoma fault (with an associated aeromagnetic anomaly). Given that several active faults in the Puget Lowland trend in a northwest-southeast direction, increased erosion along more highly fractured Quaternary deposits with similar trends is a plausible explanation for the origins of some of the valleys. Booth and others (2004) mapped gentle folds in Quaternary deposits exposed along the Puget Sound coastline between Seattle and Tacoma. Most of the fold axes trend east-west, some trend northwest-southeast, and others trend in other directions. Comparison of fold axis to upland lineations has not been done. Similar folding may be present in the Quaternary deposits north of Seattle, and if present may exert some control on drainage patterns. Additional study of such valley lineations, however, is needed to determine probable origins.

Although associated with topography in some places, we do not believe magnetic terrain causes the entire Cottage Lake aeromagnetic lineament for three reasons. (1) Measurements of magnetic susceptibility at five locations along the Cottage Lake aeromagnetic lineament indicate average induced magnetizations within Pleistocene glacial deposits ranging from 0.05 to 0.12 A/m (Table 1), sufficient to contribute to but not entirely explain the anomaly. This is further demonstrated in Figure 13C, which shows the aeromagnetic anomaly that would be caused solely by glacial terrain with a uniform magnetization of 0.08 A/m (the average of all values in Table 1). Correlations between topographic anomalies and aeromagnetic lineaments are evident in Figure 13C, but the amplitudes of these anomalies are lower than actually observed in the original data (Figure 5). (2) The altitude of the aircraft above terrain (Figure 13B), as determined by onboard radar altimetry, shows little correlation with the Cottage Lake aeromagnetic lineament. (3) Matched filter analysis (Figure 11, Table 2) indicates significant sources lying deeper than 1 km below the topographic surface.

Figure 29 shows a hypothetical geologic cross section across the Cottage Lake aeromagnetic lineament based on the aeromagnetic data. This model includes three magnetic layers: (1) weakly magnetized Pleistocene glacial deposits at the topographic surface; (2) a weakly magnetized sedimentary layer at 1 to 2 km depth, interpreted to be either Eocene volcanic rocks of Mount Persis or tuffaceous beds within the Oligocene Blakeley Formation; and (3) a highly magnetic volcanic unit beginning at 2-km depth, possibly basalts of the Eocene Crescent Formation or Eocene sandstone of Scow Bay. Although the modeled cross-section includes a north-side-up offset of magnetic layers, this is but one mathematically acceptable interpretation; an infinite variety of cross sections can be developed that satisfy the same magnetic data with equal precision. We did not attempt to constrain the dip of the fault with any precision.

The north-side up scarps (Figures 15) and apparent north-side-up offsets of magnetic layers (Figures 5, 7, 9-11, 29) are in general agreement with the regional framework of the SWIF as observed on and around Whidbey Island. Johnson and others (1996) found evidence for three strands of the SWIF in seismic-reflection data from Possession Sound (Figures 2). The northern and southern strands dip steeply northward and exhibit north-side-up displacement, whereas the central strand dips steeply southward and has its south side up. They interpreted this geometry as an antiformal flower structure, with the central strand rooting into the southern strand. In addition, Kelsey and others (2004) interpreted differences in sea-level histories at two marshes located on opposite sides of one strand of the SWIF on Whidbey Island as evidence for north-side-up displacement about 3000 years ago.

The SWIF is mapped in areas where Quaternary deposits are exposed at the ground surface, but these faults do not appear to have caused enough recent offset to juxtapose different Quaternary deposits. The hypothesized extension of the SWIF onto the mainland is thus similar to the Tacoma fault in that no apparent Quaternary stratigraphic offsets are present on the landscape. This is unlike the Seattle fault, however, where an earthquake 1100 years ago left readily apparent topographic features at the modern ground surface, and where sufficient offset has accumulated over time to produce an east-west lineation of bedrock outcrops exposed through the otherwise continuous Quaternary cover in the Puget Lowland.

Current models infer that the direction of permanent crustal shortening in central Puget Sound is approximately north-south. Regional kinematics, earthquake focal mechanisms, and fault slip data from trenches across the Seattle fault indicate north-south shortening, with little strike-slip motion (Wells and others, 1998; Nelson and others, 2003). If the same strain field characterizes the SWIF, we would expect dextral thrust motion based on the northwest trend of the fault. However, a trench across the west-northwest-trending Utsalady fault on northern Whidbey Island (Johnson and others, 2003) indicates sinistral-thrust slip during its last earthquake, inconsistent with the central Puget Sound data, but consistent with GPS shortening in the northeast direction of convergence (for example, Miller and others, 2001). The sinistral slip implies that the partitioning of the margin-parallel (north-directed) component of convergence decreases northward between Seattle and the San Juan Islands. If sinistral slip is typical of northern Puget Sound faults, the SWIF may occupy a transition zone between two different strain regimes, and may have thrust motion, with an increasing dextral component southward.

Aeromagnetic anomalies alone cannot be used to determine the age of latest deformation or rate of earthquake recurrence. If our speculations are correct (Figure 29), the Cottage Lake aeromagnetic lineament represents an offset of Pleistocene glacial deposits, Eocene and/or Oligocene sedimentary rocks, and possibly Eocene Crescent Formation. However, magnetic models are not unique, and the shallowest deformation in the Alderwood #1 well is recorded at 1209 m depth (Standard Oil Company of California report, 1947), which falls within late Eocene to early Oligocene Blakeley Formation, as interpreted by Rau and Johnson (1999). Thus, if the Cottage Lake aeromagnetic lineament reflects deformation, we can only state with confidence that it must have occurred more recently than about 35 Ma. Trench excavations across the scarps near Crystal and Cottage Lakes are needed to determine if the scarps have a tectonic origin and, if so, further constrain the recency of surface deformation. Ongoing studies of data from boreholes recently drilled as part of a proposed wastewater conveyance project may

provide additional evidence to evaluate the possibility of tectonic disruption of near-surface soils.

CONCLUSIONS

We have tested the hypothesis that the SWIF extends southeastward from Whidbey Island to the mainland region between Snohomish and Lake Washington. The Cottage Lake and other northwest-trending aeromagnetic lineaments reflect northwest-trending geologic structures between Snohomish and Lake Washington. The geometry and locations of these structures are consistent with those one might expect from the hypothesized southeastward extension of the SWIF onto the mainland. Evidence of subsurface deformation and disturbance is present in boreholes and in one deep well and suggests a structural origin for some of the anomalies. Most subsurface disturbance observed within the boreholes occurred prior to 15-13 ka; deformation within the deep well can only be constrained as post-early Oligocene and pre-Pleistocene. Subtle, discontinuous, post-glacial topographic scarps visible on lidar images coincide with the aeromagnetic lineament over a distance of 18 km. The scarps exhibit variable morphology and cut across the glacial flutes at an acute angle. Although they may have various origins, the coincidence between the subsurface-generated magnetic anomalies and surface disturbance suggests a possible tectonic origin. In summary, the Cottage Lake aeromagnetic lineament is the most likely location of a hypothetical projection of the SWIF. This hypothesis can be further tested with paleoseismic studies of identified scarps.

ACKNOWLEDGMENTS

We are indebted to the Puget Sound Lidar Consortium for providing the lidar topographic data collected by King County. We are grateful to King County for allowing us to present the borehole data and to the CDM Brightwater conveyance team for their borehole analysis. We appreciate advance comments from Derek Booth, Tom Brocher, and Bob Yeats which helped refine some of our discussion, and we are indebted to Tom Brocher, Vicki Langenheim, and Alan Nelson for technical review of our manuscript and for critical comments.

REFERENCES

Baranov, V., 1957, A new method for interpretation of aeromagnetic maps: pseudo-gravimetric anomalies: Geophysics, v. 22, p. 359-383.

Bates, R.L., and Jackson, J.D., eds., 1980, Glossary of Geology (2 ed.): Falls Church, Virginia, American Geological Institute, 751 p.

Blakely, R.J., 1995, Potential Theory in Gravity and Magnetic Applications: Cambridge University Press, 441.

Blakely, R.J., and Simpson, R.W., 1986, Approximating edges of source bodies from magnetic or gravity anomalies: Geophysics, v. 51, p. 27-40.

Blakely, R.J., Wells, R.E., and Weaver, C.S., 1999, Puget Sound aeromagnetic maps and data: U.S. Geological Survey Open-File Report 99–514, http://geopubs.wr.usgs.gov/open-file/of99-514.

Blakely, R.J., Wells, R.E., Weaver, C.S., and Johnson, S.Y., 2002, Location, structure, and seismicity of the Seattle fault zone, Washington: Evidence from aeromagnetic anomalies, geologic mapping, and seismic-reflection data: Geological Society of America Bulletin, v. 114, p. 169-177.

Booth, D.B., and Hallet, B., 1993, Channel networks carved by subglacial water: Observations and reconstruction in the eastern Puget Lowland of Washington: Geological Society of America Bulletin, v. 105, p. 671–683.

Booth, D.B., Haugerud, R.A., and Troost, K.G., 2003, Geology, Watersheds, and Puget Lowland Rivers, p. 14-45, in Montgomery, D. M., Bolton, S., and Booth, D. B., eds., 2003, Restoration of Puget Sound Rivers: Seattle, Society for Ecological Restoration, University of Washington Press, 505 pp.

Booth, D.B., Troost, K.G., and Hagstrum, J.T., 2004, Deformation of Quaternary strata and its relationship to crustal folds and faults, central Puget Lowland, Washington: Geology, v. 32 (in press).

Brocher, T.M., Blakely, R.J., and Wells, R.E., 2004, Interpretation of the Seattle uplift, Washington, as a passive roof duplex: Bulletin of the Seismological Society of America, in press.

Brocher, T.M., Parsons, R.J., Blakely, R.J., Christensen, N.I., Fisher, M.A., Wells, R.E., and the SHIPS Working Group, 2001, Upper crustal structure in Puget Lowland, Washington: Results from the 1998 Seismic Hazards Investigation in Puget Sound: Journal of Geophysical Research, v. 106, p. 13,541–13,564.

Bucknam, R.C., Hemphill-Haley, E., and Leopold, E.B., 1992, Abrupt uplift within the past 1700 yr at southern Puget Sound, Washington: Science, v. 258, p. 1611-1614.

CDM, 2004, Predesign Geotechnical Data Report, Conveyance System: A King County Brightwater Project report prepared by CDM, Bellevue, Washington, February, 2004.

Finn, C., 1990, Geophysical constraints on Washington Convergent margin structure: Journal of Geophysical Research, v. 95, p. 19,533-19,546.

Goldstein, B.S., 1994, Drumlins of the Puget Lowland, Washington State, USA: Sedimentary Geology, v. 91, no. 1-4, p. 299-311.

Gower, H.D., Yount, J.C., and Crosson, R.S., 1985, Seismotectonic map of the Puget Sound region, Washington: U.S. Geological Survey Miscellaneous Investigations Map I-1613, scale 1:250,000.

Grauch, V.J.S., Hudson, M.R., and Minor, S.A., 2001, Aeromagnetic expression of faults that offset basin fill, Albuquerque basin, New Mexico: Geophysics, v. 66, p. 707-720.

Haugerud, R.A., Harding, D.J., Johnson, S.Y., Harless, J.L., Weaver, C.S., and Sherrod, B.L., 2003, High-resolution Lidar topography of the Puget Lowland, Washington: GSA Today, v. 13, p. 4-10.

Hyndman R. D., S. Mazzotti, D. Weichert, and G. C. Rogers, Frequency of large crustal earthquakes in Puget Sound-Southern Georgia Strait predicted from geodetic and geological deformation rates: Journal of Geophysical Research, v. 108 (B1), p. 2033, doi:10.1029/2001JB001710, 2003.

Johnson, S.Y., Dadisman, S.V., Mosher, D.C., Blakely, R.J., and Childs, J.R., 2001, Active tectonics of the Devils Mountain fault and related structures, northern Puget Lowland and eastern Strait of Juan de Fuca region, Pacific Northwest: U.S. Geological Survey Professional Paper 1643, 45 p., 2 plates.

Johnson, S.Y., Nelson, A.R., Personius, S.F., Wells, R.E., Kelsey, H.M., Sherrod, B.L., Okumura, K., Koehler, R., Witter, R., Bradley, L.-A., Harding, D.J., 2003, Maps and data from a trench investigation of the Utsalady Point fault, Whidbey Island, Washington: U.S. Geological Survey Miscellaneous Field Investigations MF-2420, 1 sheet.

Johnson, S.Y., Potter, C.J., Armentrout, J.M., Miller, J.J., Finn, C., and Weaver, C.S., 1996, The southern Whidbey Island fault: An active structure in the Puget Lowland, Washington: Geological Society of America Bulletin, v. 108, p. 334-354, 1 insert.

Kelsey, H.M., Sherrod, B., Johnson, S.Y., and Dadisman, S.V., 2004, Land-level changes from a late Holocene earthquake in the northern Puget lowland, Washington: Geology, in press.

Miller, M.M., Johnson, D.J., Rubin, C.M., Dragert, H., Wang, K., Qamar, A., Goldfinger, C., 2001, GPS-determination of along-strike variation in Cascadia margin kinematics: Implications for relative plate motion, subduction zone coupling, and permanent deformation: Tectonics, v. 20, p. 161-176.

Minard, J.P., 1985, Geologic map of the Maltby quadrangle, Snohomish and King Counties, Washington: U.S. Geological Survey Miscellaneous Field Studies Map MF-1746, scale 1:24,000.

Nelson, A.R., Johnson, S.Y., Kelsey, H.M., Wells, R.E., Sherrod, B.L., Pezzopane, S.K., Bradley, L., Koehler, R.D., and Bucknam, R.C., 2003, Late Holocene earthquakes on the Toe Jam Hill fault, Seattle fault zone, Bainbridge Island, Washington: Geological Society of America Bulletin, v. 115, p. 1388-1403.

Phillips, J.D., 1997, Potential-field geophysical software for the PC, version 2.2: U.S. Geological Survey Open-File Report 97-725, 34 p.

Ponce, D.A., and Glen, J.M.G., 2002, Relationship of epithermal gold deposits to large-scale fractures in northern Nevada: Economic Geology, v. 97, p. 3-9.

Ponce, D.A., Hildenbrand, T.G., and Jachens, R.C., 2003, Gravity and magnetic expression of the San Leandro gabbro with implications for the geometry and evolution of the Hayward fault zone, northern California: Bulletin of the Seismological Society of America, v. 93, p. 14-26.

Porter, S.C., and Swanson, T.W., 1998, Radiocarbon age constraints on rates of advance and retreat of the Puget lobe of the Cordilleran ice sheet during the last glaciation: Quaternary Research, v. 50, p. 205-213.

Rau, W.W., and Johnson, S.Y., 1999, Well stratigraphy and correlations, western Washington and northwestern Oregon: U.S. Geological Survey Geologic Investigations Series Map I-2621, 31 pages, 3 foldouts.

Sherrod, B.L., Brocher, T.M., Weaver, C.S., Bucknam, R.C., Blakely, R.J., Kelsey, H.M., Nelson, A.R., and Haugerud, R., 2004, Holocene fault scarps near Tacoma, Washington, USA: Geology, v. 32, p. 9-12.

Sherrod, B.L., 2002, Late Quaternary surface rupture along the Seattle fault zone near Bellevue, Washington: EOS Transactions of the American Geophysical Union, v. 83, n. 47, Fall Meeting Supplement, Abstract S21C-12.

Spector, A., and Grant, F.S., 1970, Statistical models for interpreting aeromagnetic data: Geophysics, v. 35, p. 293-302.

Syberg, F.J.R., 1972, A Fourier method for the regional-residual problem of potential fields: Geophysical Prospecting, v. 20, p. 47-75.

Tabor, R.W., Frizzell, V.A., Jr., Booth, D.B., Waitt, R.B., Jr., Whetten, J.T., and Zartman, R.E., 1993, Geologic map of the Skykomish River 30- by 60-minute quadrangle, Washington: U.S. Geological Survey Map I-1963, scale 1:100,000.

Telford, W.M., Geldart, L.P., and Sheriff, R.E., 1990, Applied Geophysics Second Edition: Cambridge University Press, 770 p.

Yount, J.C., and Gower, H.D., 1991, Bedrock geologic map of the Seattle 30’ by 60’ quadrangle, Washington: U.S. Geological Survey Open-File Report 91-147, 37 p. 4 plates, scale 1:100,000.

Wells, R.E., and Simpson, R.W., 2001, Northward migration of the Cascadia forearc in the northwestern U.S. and implications for subduction deformation: Earth, Planets, and Space, v. 53, p. 275-283.

Wells, R.E., Weaver, C.S., and Blakely, R.J., 1998, Fore-arc migration in Cascadia and its neotectonic significance: Geology, v. 26, p. 759-762.

Table 1.—Magnetic susceptibility measurements in the Woodinville-Maltby area. All measurements conducted with a hand-held Model KT-6 Kappameter manufactured by Geofyzika.

Location	Description	Susc.[1]	N[2]	Magn.[3]
NE 160th St and 210th Ave NE	Pleistocene glacial deposit	2.817	10	0.12
NE 159th St and 202nd Ave NE	Pleistocene glacial deposit	1.832	10	0.08
NE 205th St	Pleistocene glacial deposit	1.367	10	0.06
NE 205th St	Pleistocene glacial deposit	1.335	10	0.05
NE 205th St	Pleistocene glacial deposit	2.405	8	0.11
Welch Rd near Elliott Rd	Blakeley Formation, fine grained	0.225	10	0.01
Welch Rd near Elliott Rd	Blakeley Formation, pebbly	2.690	13	0.11
Welch Rd near Elliott Rd	Blakeley Formation, fine grained	0.150	3	0.01
Elliott Rd near Fales Rd	Blakeley Formation, fine grained	0.308	16	0.01
SR 522 near Bald Hill, site A	Mt. Persis volc. rocks, weathered	2.173	19	0.10
SR 522 near Bald Hill, site B	Mt. Persis volc. rocks, unweathered	16.894	14	0.75
Gravel pit, Snohomish-Monroe Rd	Mt. Persis volc. rocks, weathered	5.255	17	0.23
Quarry on Bald Hill	Mt. Persis volc. rocks, unweathered	16.160	10	0.71

[1] Average susceptibility in SI units; displayed numbers multiplied by 10^3

[2] Number of individual measurements

[3] Magnetization in A/m

Table 2.—Interpretation of matched-filter analysis of aeromagnetic anomalies of the region between Mukilteo and Lake Washington. Analysis covers the area shown in Figure 11.

Layer	Depth[1] (m)	Amplitude (nT)	Interpretation
1	107	$2.67x10^{-5}$	Located above ground level. Noise caused by minor fluctuations in aircraft altitude, small errors in navigation, etc.
2	433	$8.66x10^{-3}$	Very weakly magnetic glacial and interglacial deposits and Blakeley Formation
3	1245	0.14	Weakly magnetic sedimentary or volcanic rocks, possibly tuffaceous units within the Blakeley Formation or volcanic rocks of Mt. Persis
4	2723	1.43	Crescent Formation and/or sandstone of Scow Bay

[1] Relative to aircraft altitude.

Table 3.—Features identified in GIS analysis of lidar data from northern King County and southern Snohomish County.

Feature No.	Feature type	Possible Interpretation	Confidence of Interpretation	Field Checked
1	lineament	structural lineament	medium	no
2	lineament	structural lineament	medium	no
3	lineament	structural lineament	medium	yes
4	lineament	structural lineament	medium	yes
5	lineament	structural lineament	medium	no
6	scarp	fault scarp	medium	no
7	lineament	structural lineament	medium	yes
8	scarp	fault or landslide scarp	high	yes
9	scarp	fault or landslide scarp	low	no
10	scarp	fault scarp	high	yes
11	possible scarp	fault scarp	medium	yes
12	scarp	landslide scarp	medium	no
13	scarp	landslide or fault scarp	low	no
14	scarp/lineament	structural lineament	low	no
15	scarp	fault scarp	high	yes
16	scarp	en-echelon fault scarp	medium	yes
17	scarp	fault scarp	medium	yes
18	scarp	fault scarp	high	yes
19	lineament	structural or glacial lineament	low	no
20	lineament	structural or glacial lineament	low	no
21	possible scarp	post-glacial channel edge	medium	no

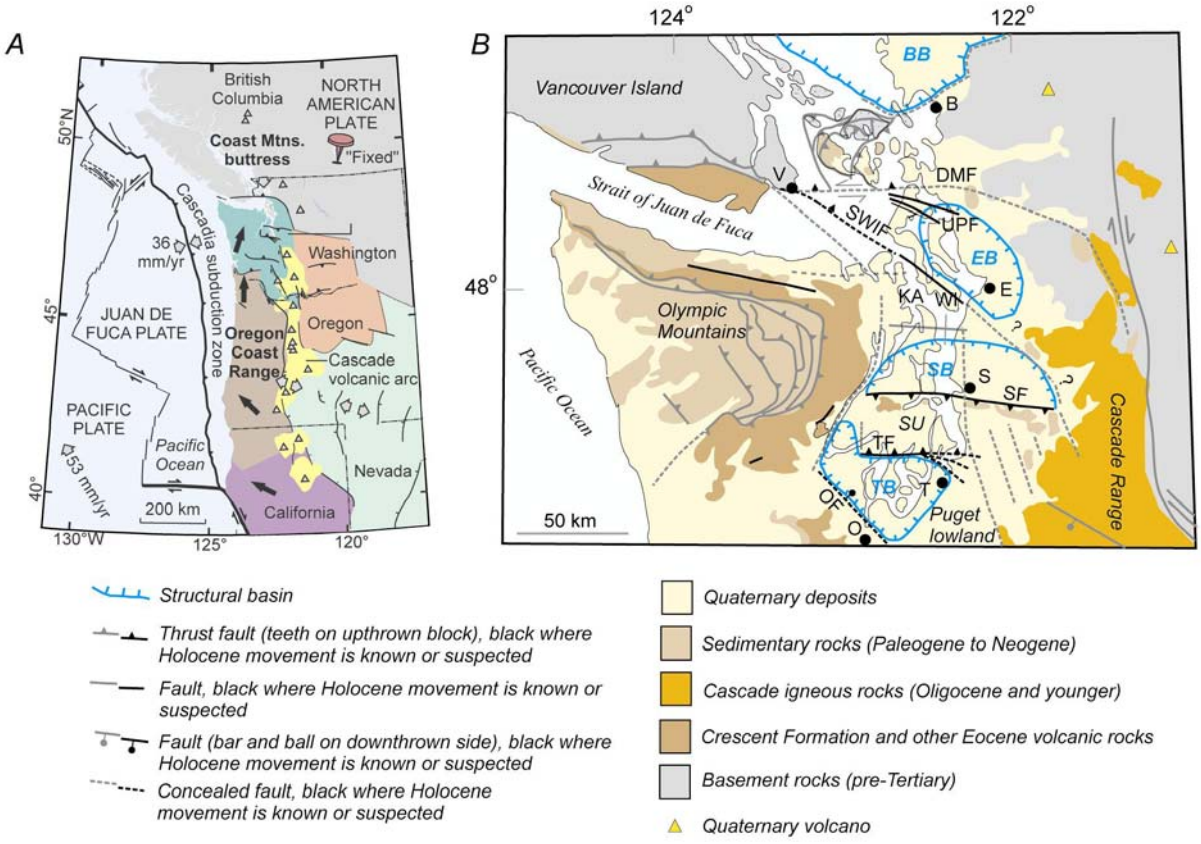

Figure 1.-(A) Kinematic model of the Cascadia forearc, simplified from Wells and others (1998) and Wells and Simpson (2001). Northward motion of Oregon microplate (large black arrows) squeezes western Washington against fixed North America, producing earthquakes and faults in Puget Lowland. (B) Generalized geologic and tectonic map of the Puget Lowland and surrounding regions. BB, Bellingham basin; EB, Everett basin; SB, Seattle basin; TB, Tacoma basin; DMF, Devils Mountain fault; UPF, Utsalady Point fault; SWIF, southern Whidbey Island fault; SF, Seattle fault; TF, Tacoma fault; OF, Olympia fault; V, Vancouver; B, Bellingham; E, Everett; S, Seattle; T, Tacoma; O, Olympia; WI, Whidbey Island; KA, Kingston arch; SU, Seattle uplift.

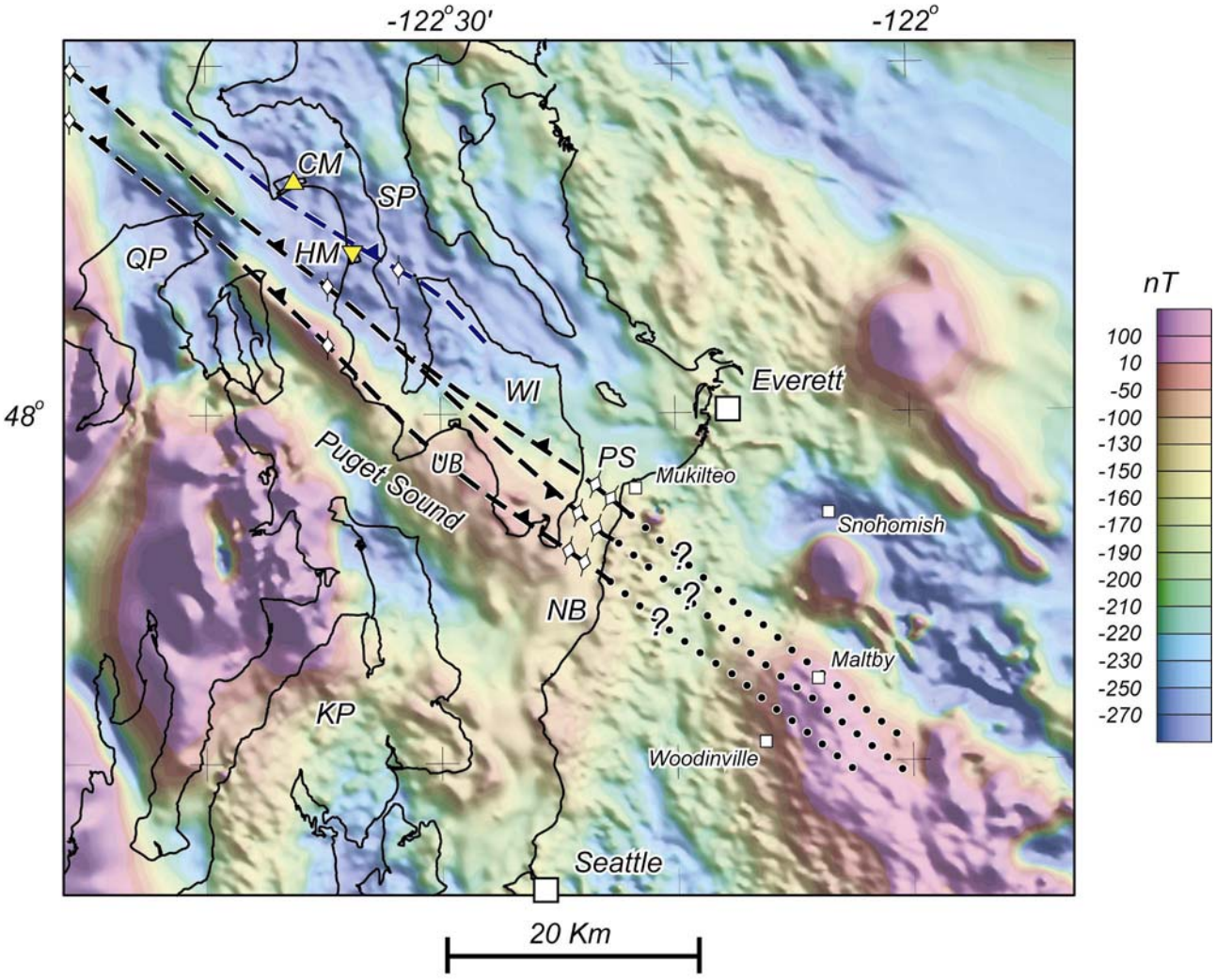

Figure 2.-Evidence for the SWIF on Whidbey Island. Color-shaded relief image indicates intensity of magnetic field observed in a high-resolution aeromagnetic survey (Blakely and others, 1999). Dotted and dashed lines show faults from published reports: black lines from Johnson and others (1996), blue line from Kelsey and others (2004). White diamonds show approximate location of marine seismic-reflection evidence for Quaternary fault offsets. Yellow triangles indicate studies of relative sea-level history at two coastal marshes (Kelsey and others, 2004); northern triangle (Crockett Marsh) is up relative to southern triangle (Hancock Marsh). CM, Crockett Marsh; HM, Hancock Marsh; WI, Whidbey Island; SP, Saratoga Passage; PS, Possession Sound; QP, Quimper Peninsula; KP, Kitsap Peninsula; NB, Nora Beach.

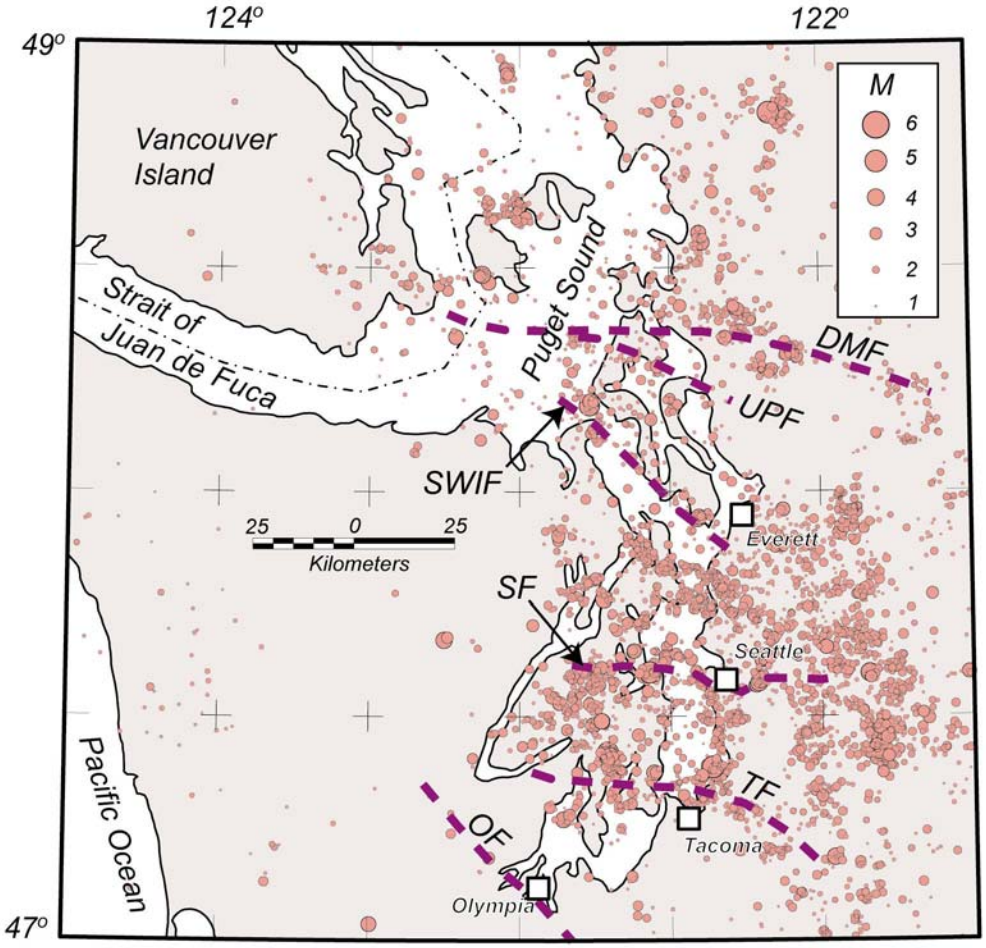

Figure 3.-Crustal earthquakes of northwestern Washington, from Pacific Northwest Seismic Network, University of Washington, 1971 through 2003. Symbol size proportional to earthquake magnitude. Bold lines indicate faults as interpreted from aeromagnetic anomalies (Figure 4). See caption to Figure 1 for label explanations.

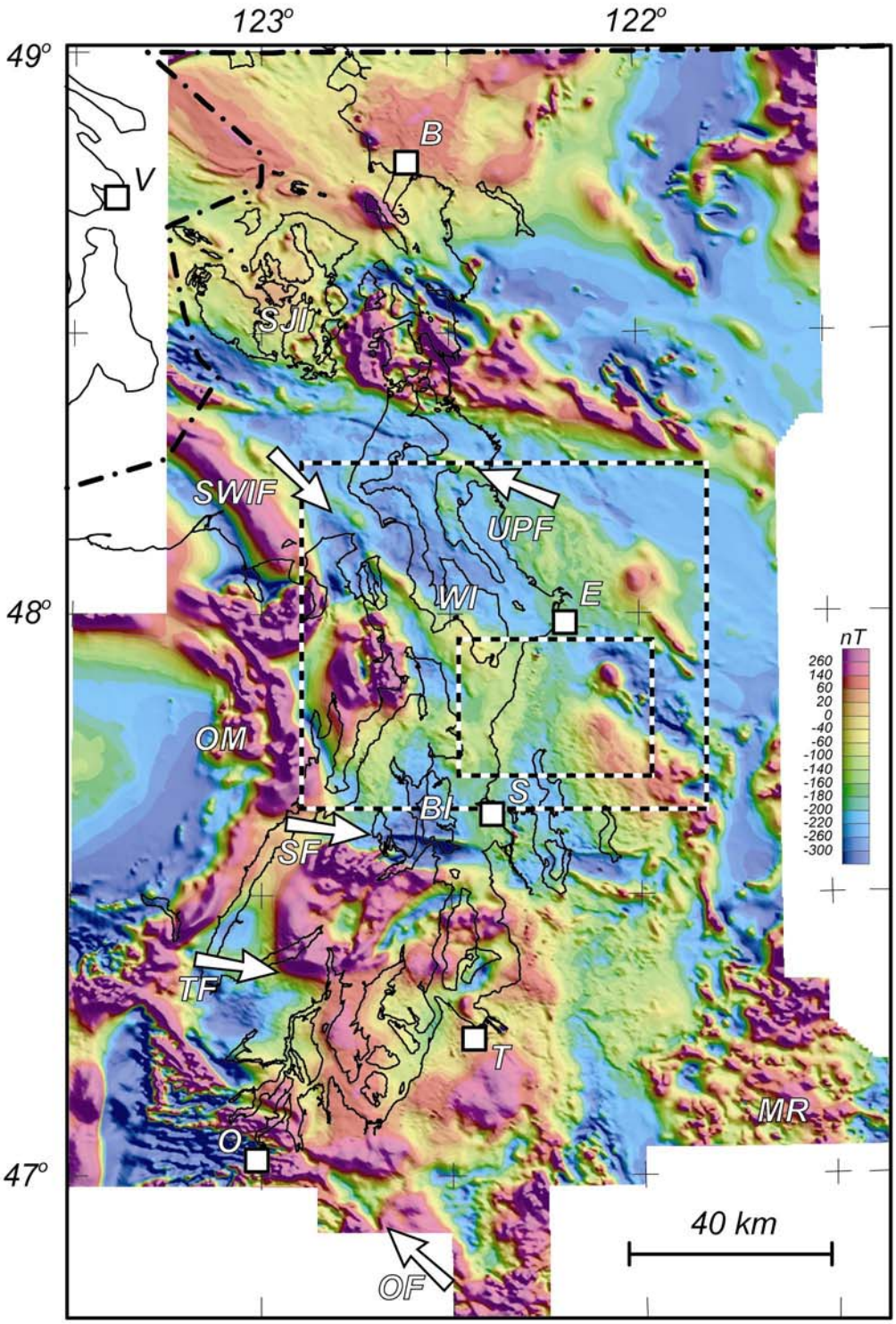

Figure 4.-Puget Lowland aeromagnetic survey. Color-shaded relief image indicates intensity of magnetic field observed in a high-resolution aeromagnetic survey (Blakely and others, 1999). Color intervals based on equal histogram algorithm. Large dashed rectangle indicates area of Figure 2; small rectangle shows study area (Figures 5, 7, 9-11, 14). SJI, San Juan Islands; BI, Bainbridge Island; MR, Mount Rainier; OM, Olympic Mountains. Arrows indicate linear anomalies associated with major crustal faults. See Figure 1 for explanation of other labels.

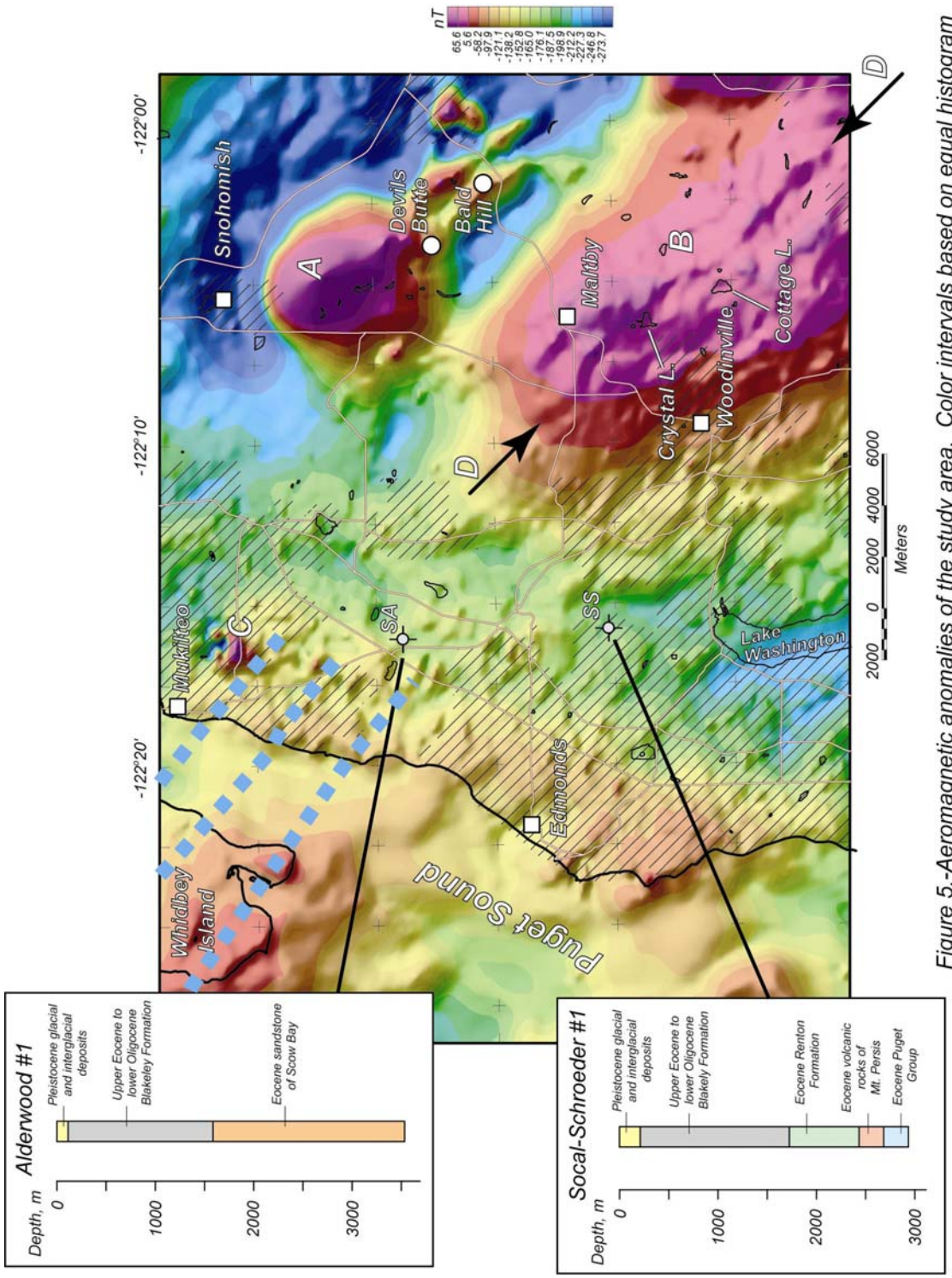

Figure 5.-Aeromagnetic anomalies of the study area. Color intervals based on equal histogram algorithm. Major roads indicated by brown lines. Black arrows and labels A, B, C, and D refer to magnetic anomalies discussed in text. Crosshatched areas are heavily urbanized. Blue dashed lines are strands of the SWIF, as interpreted by Johnson and others (1996). SA, Standard Oil Company of California Alderwood #1 well; SS, Standard Oil Company of California Socal-Schroeder #1 well. Insets: Stratigraphy of Alderwood #1 and Socal-Schroeder wells (Standard Oil Company of California), summarized from Rau and Johnson (1999).

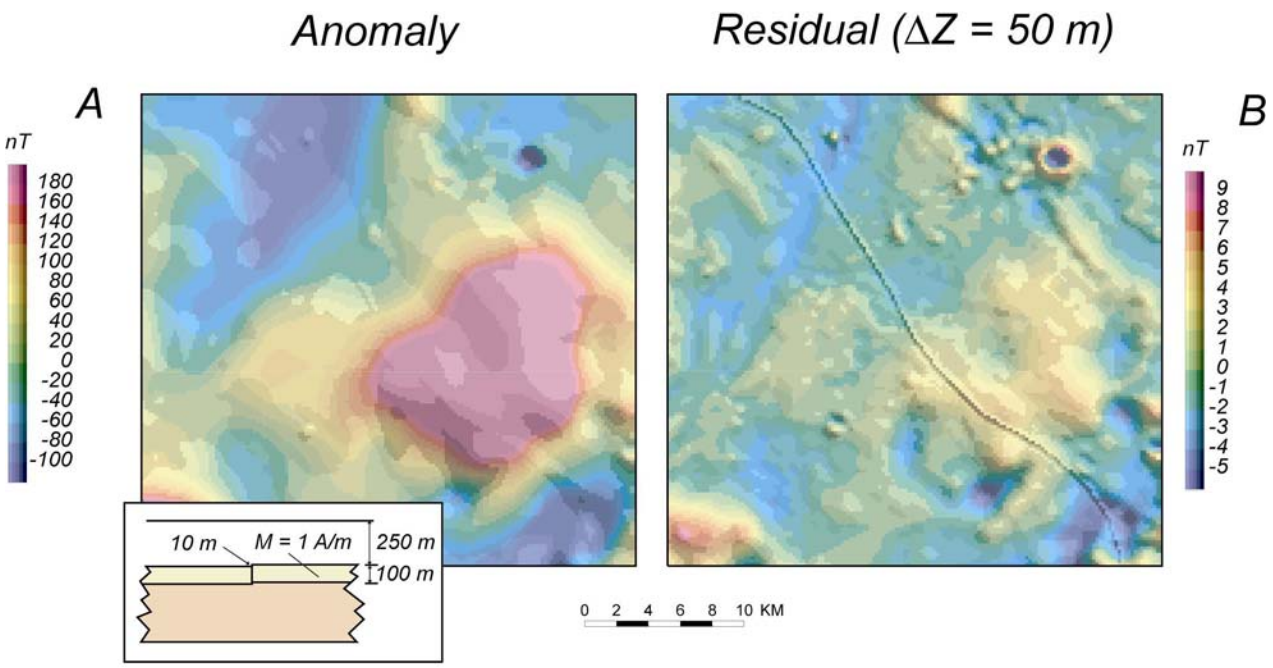

Figure 6.-Demonstration of the residual method, a way to emphasize magnetic anomalies caused by shallow sources. (A) Aeromagnetic anomalies (actually measured), plus a hypothetical anomaly caused by a small vertical offset of a shallow, weakly magnetic sedimentary layer (inset). (B) The same data as displayed in Figure 6A after application of the residual method. Upward-continuation distance 50 m.

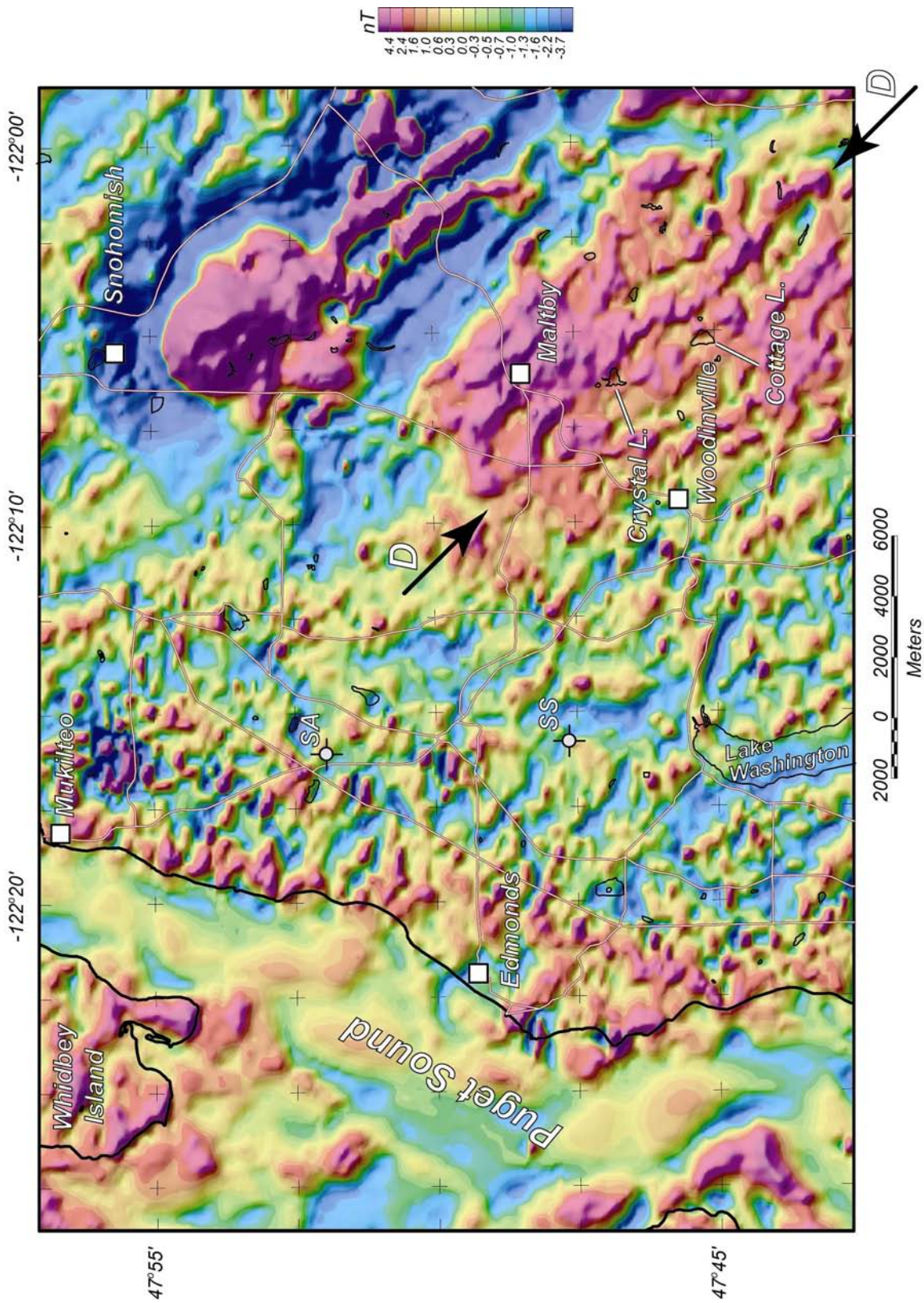

Figure 7.-Residual magnetic anomalies of the study area. Upward-continuation distance 50 m. Major roads indicated by brown lines. See Figure 5 for description of labels and symbols.

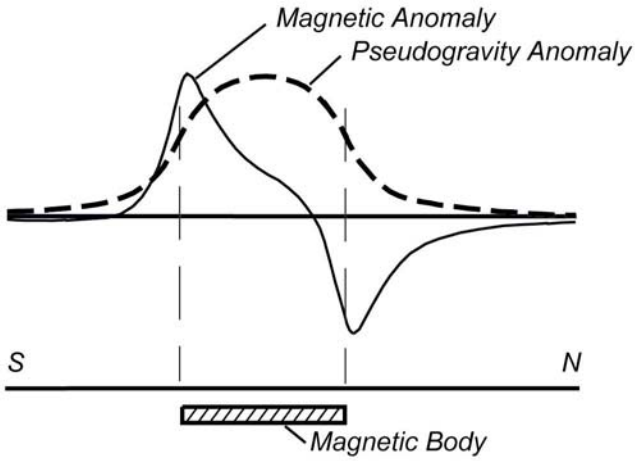

Figure 8.-Schematic illustration of a method to locate magnetic contacts from magnetic anomalies. Three steps are involved: (1) Transform magnetic anomalies to pseudogravity anomalies, (2) calculate maximum horizontal gradient, and (3) plot location of all maxima on a map. Note that the pseudogravity transformation simplifies the "dipolar" nature of the magnetic anomaly, placing steepest gradients over the edges of the causative body.

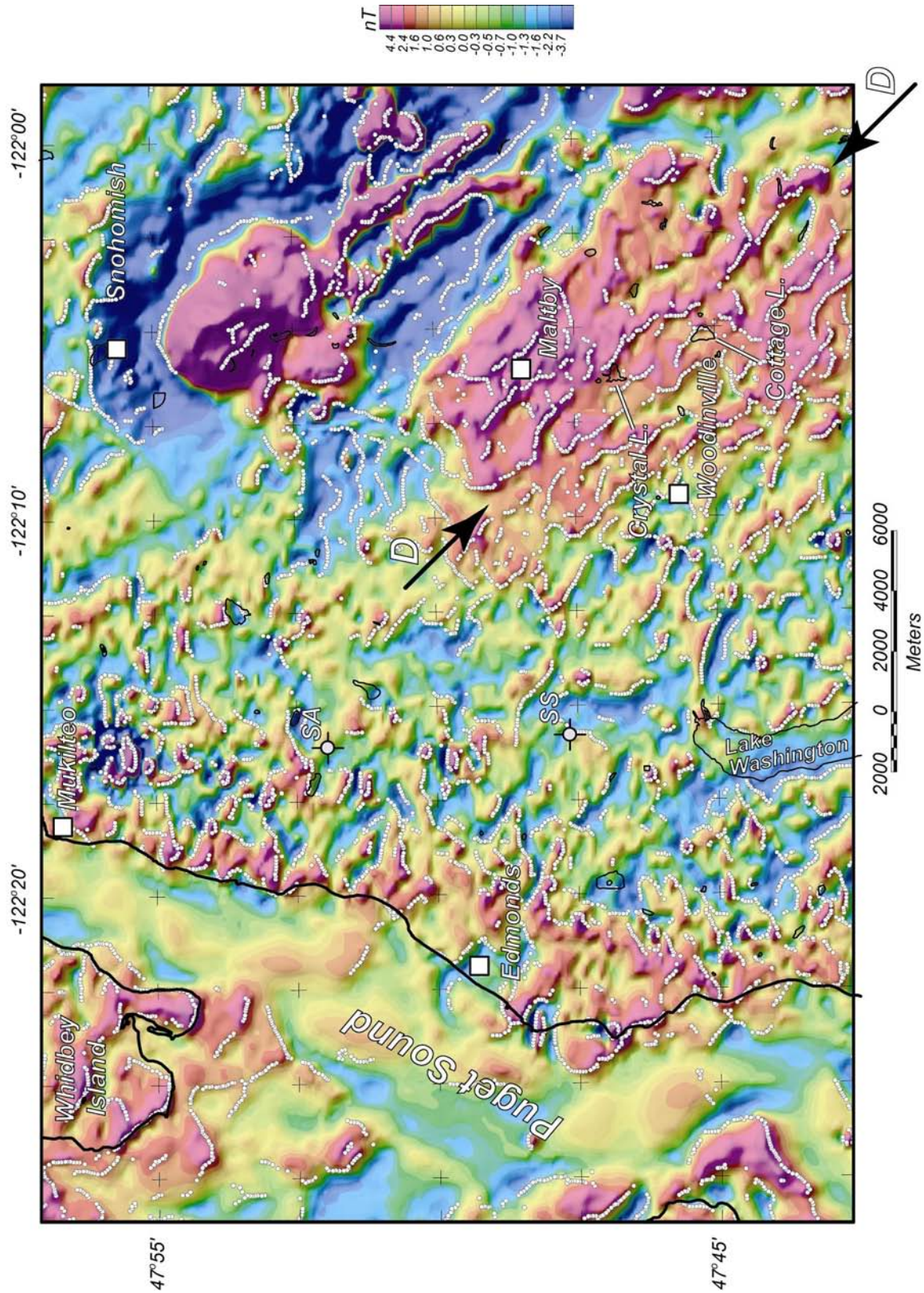

Figure 9.-Boundary analysis of magnetic anomalies of the study area. White dots show the location of magnetic contacts determined automatically with the method of Blakely and Simpson (1986). See Figure 5 for description of labels and symbols.

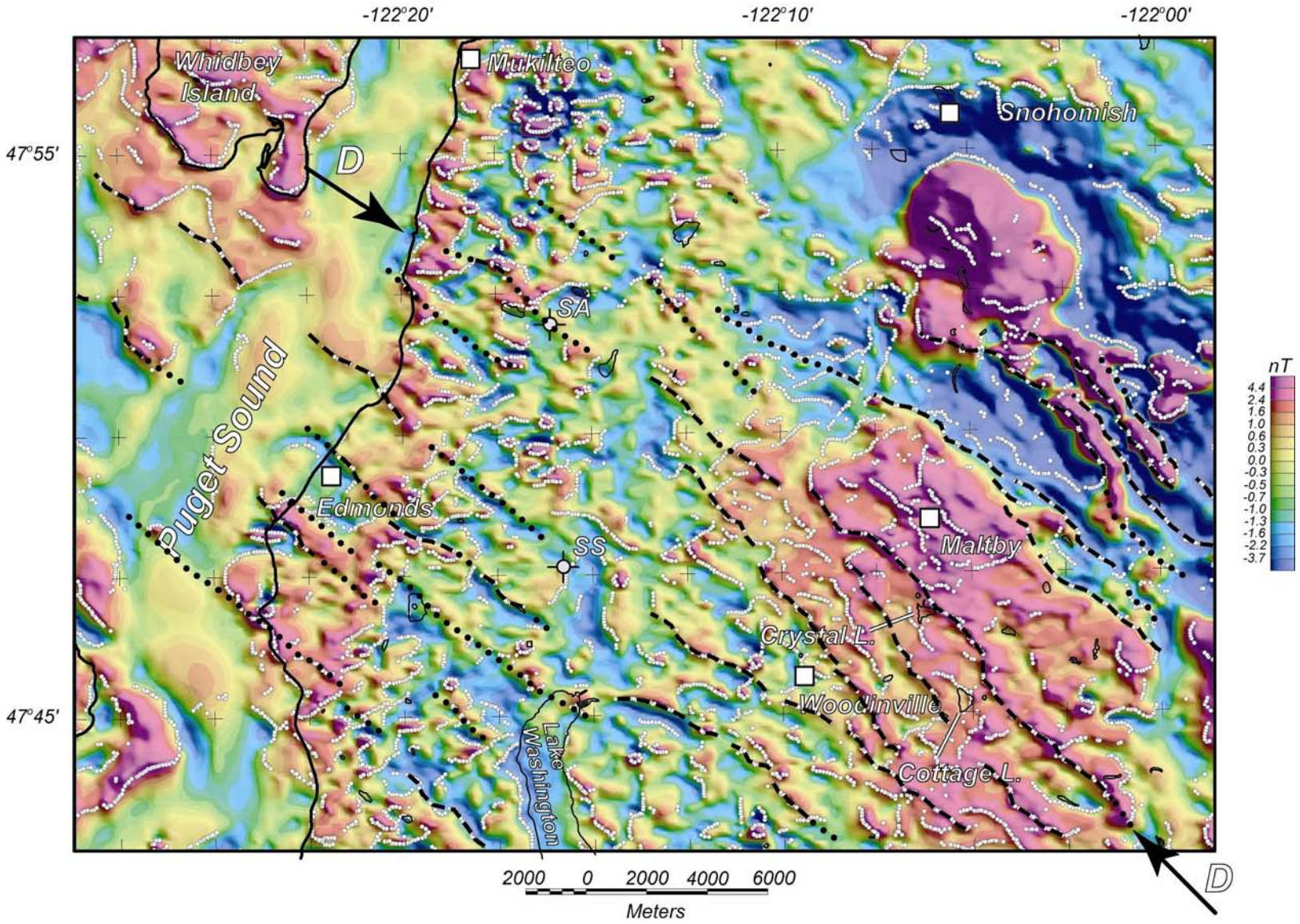

Figure 10.-Interpretation of residual aeromagnetic anomalies of the study area. Black dashed lines indicate lineaments associated with specific magnetic contrasts (white dots of Figure 7); black dotted lines are lineaments identified with lower confidence, as described in text. See label 5 for description of labels and symbols.

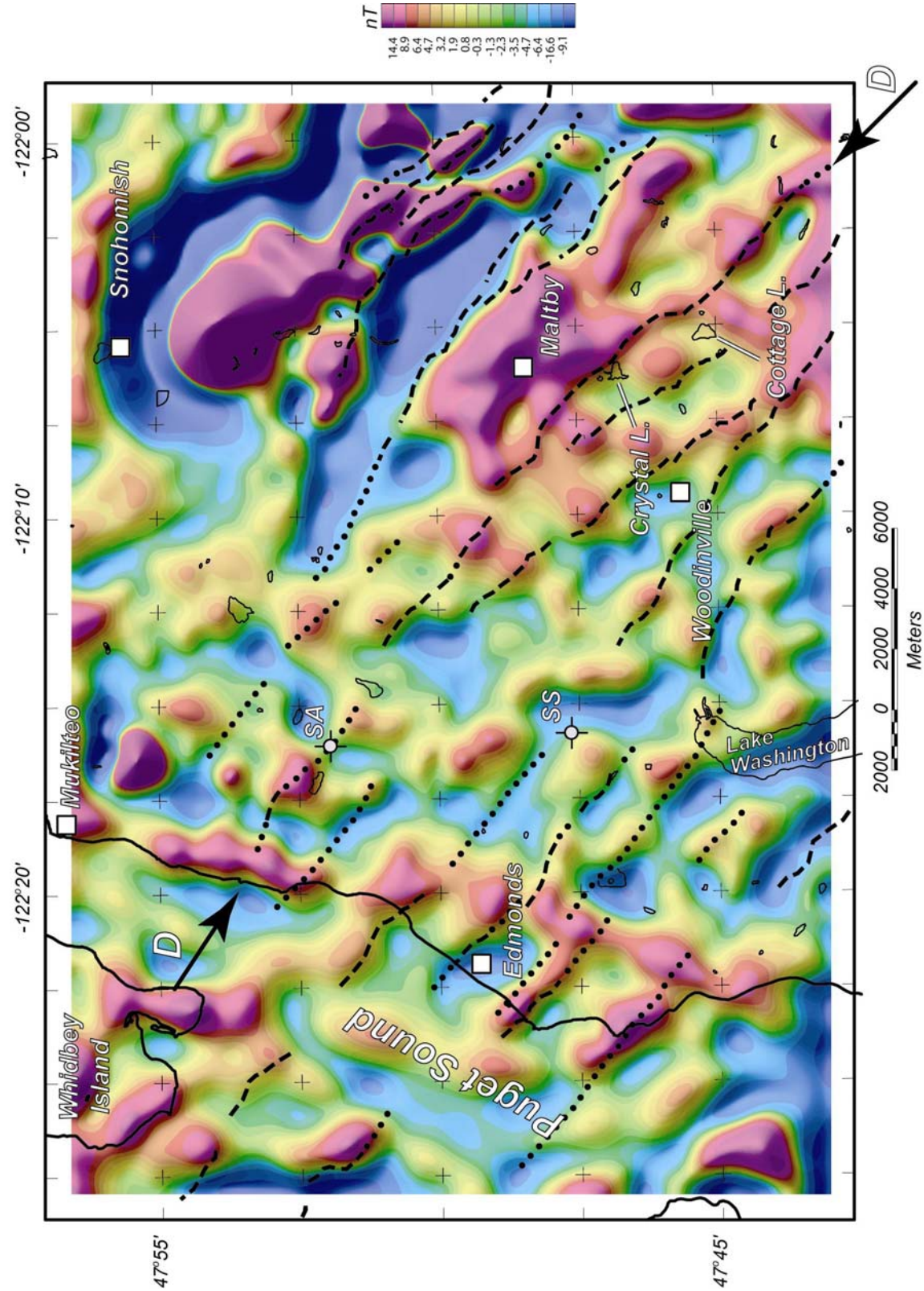

Figure 11.-Matched-filter analysis of aeromagnetic anomalies of the study area. Data shown in Figure 5 were analyzed by the method of Phillips (1997) to determine important source depths (Table 2). Based on those results, matched filters were designed to emphasize the contributions of each layer. The map shown here shows one of the intermediate-depth layers, with top at 1245 m below aircraft altitude. Dashed and dotted black lines taken from Figure 10. See Figure 5 and 10 for description of labels and symbols.

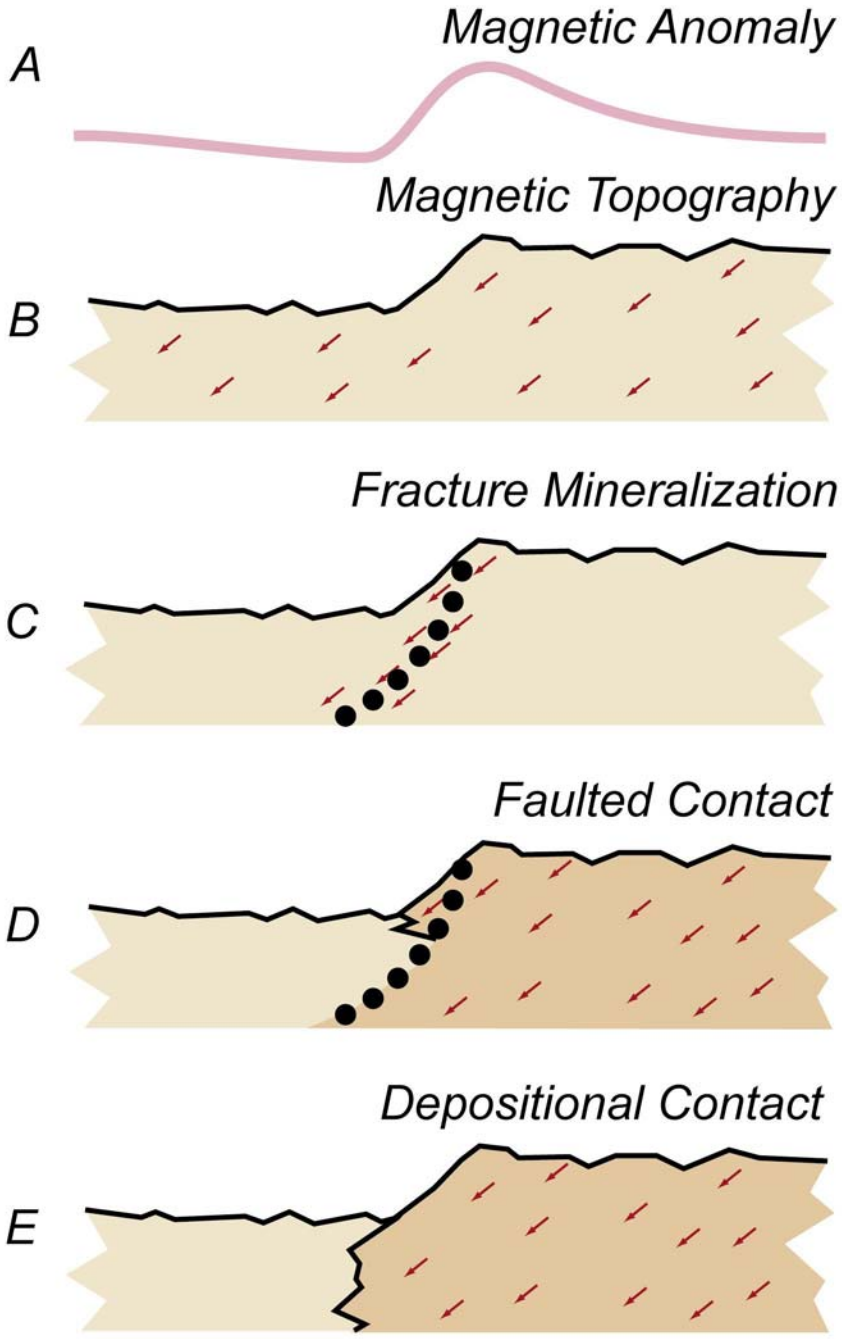

Figure 12.-Four geologic explanations for linear magnetic anomalies associated with terrain. See text for discussion.

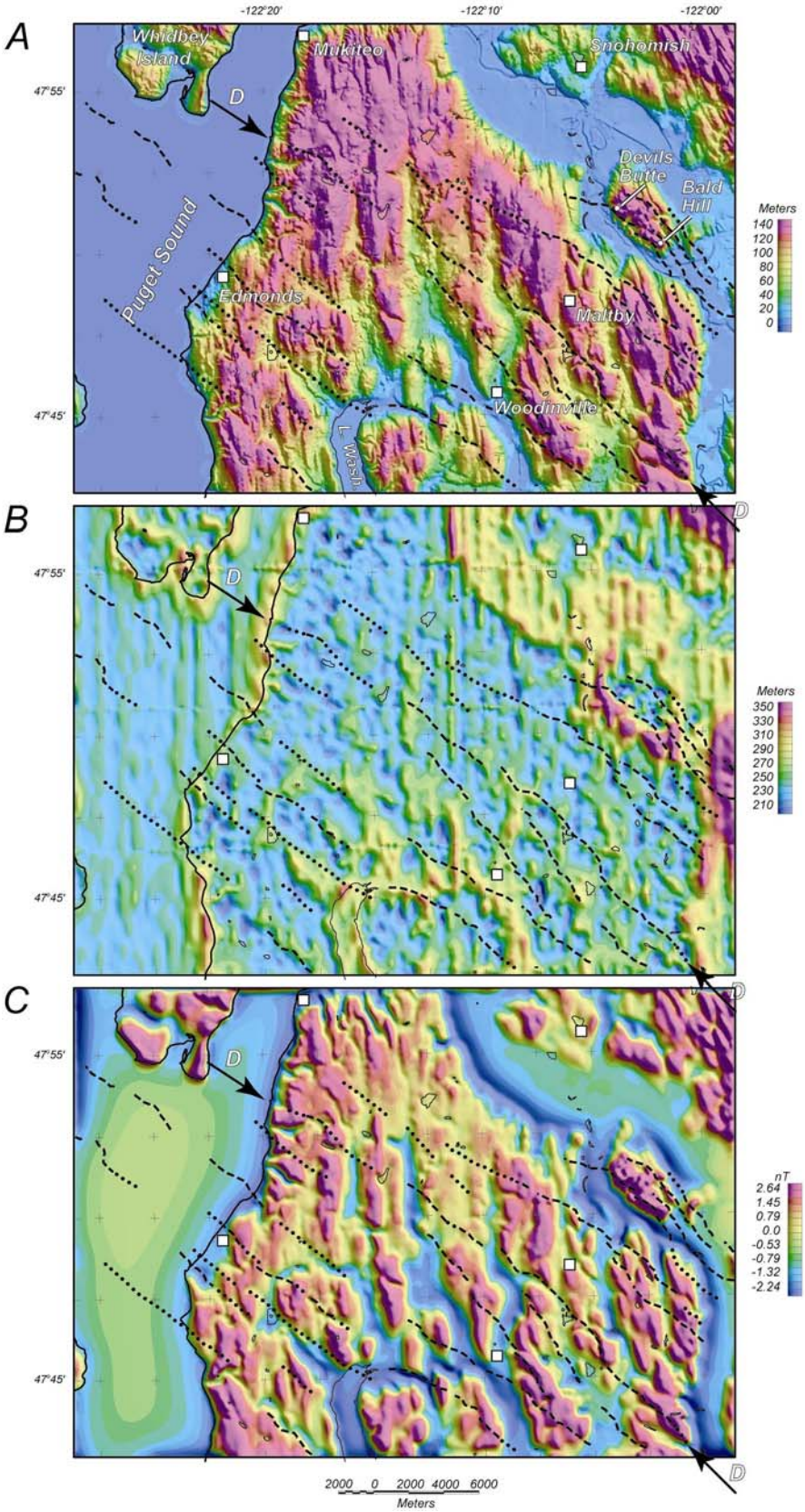

Figure 13.-(A) Topography of the study area derived from 10-m digital elevation model. (B) Altitude of aeromagnetic sensor as determined by onboard radar altimetry. (C) Calculated aeromagnetic anomaly observed on a horizontal surface assuming uniformly magnetized terrain. Flight surface assumed to be 325 m above sea level (mean of terrain clearance plus mean of terrain elevation). Inclination and declination of ambient field and magnetization 70° and 19°, respectively. Magnetization intensity 0.08 A/m. See Figures 5 and 10 for description of labels and symbols.

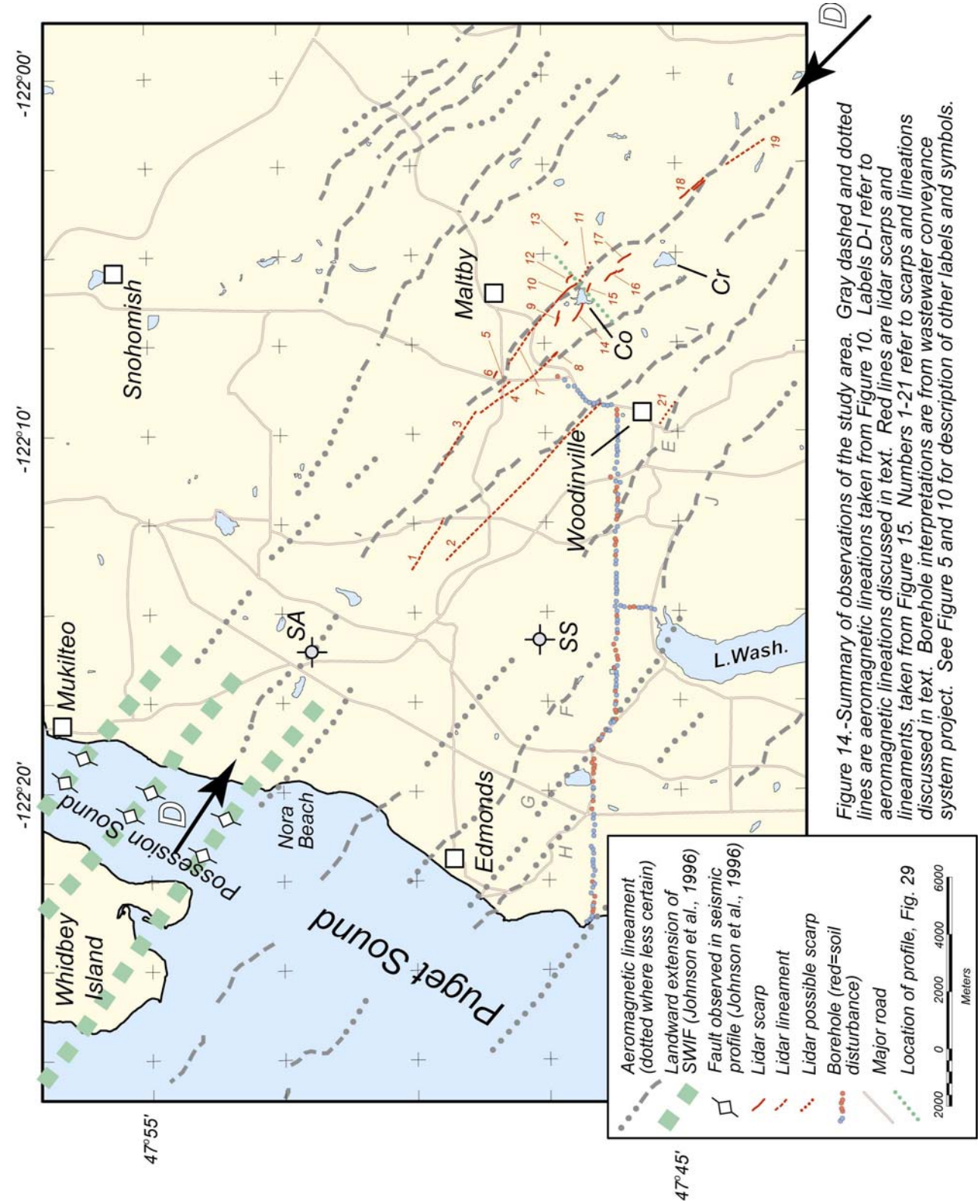

Figure 14.-Summary of observations of the study area. Gray dashed and dotted lines are aeromagnetic lineations taken from Figure 10. Labels D-I refer to aeromagnetic lineations discussed in text. Red lines are lidar scarps and lineaments, taken from Figure 15. Numbers 1-21 refer to scarps and lineations discussed in text. Borehole interpretations are from wastewater conveyance system project. See Figure 5 and 10 for description of other labels and symbols.

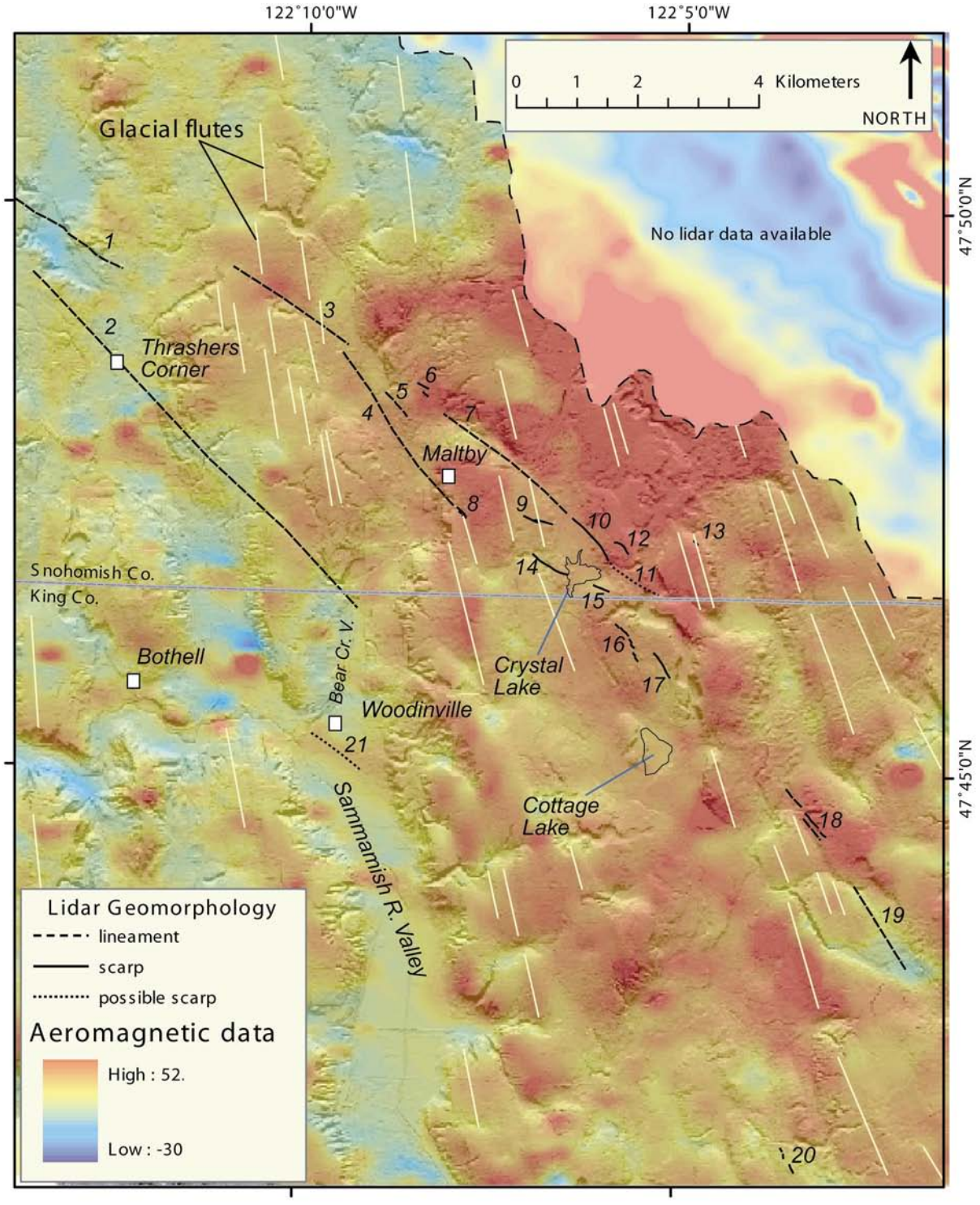

Figure 15.-(A) Lidar map of Cottage Lake aeromagnetic lineament, with a gridded layer of residual aeromagnetic data draped over the lidar data as a transparent colored image. Numbered solid and dashed lines show locations of topographic features identified on the lidar maps and referred to in the text and Table 3. Pale lines indicate glacial flute directions.

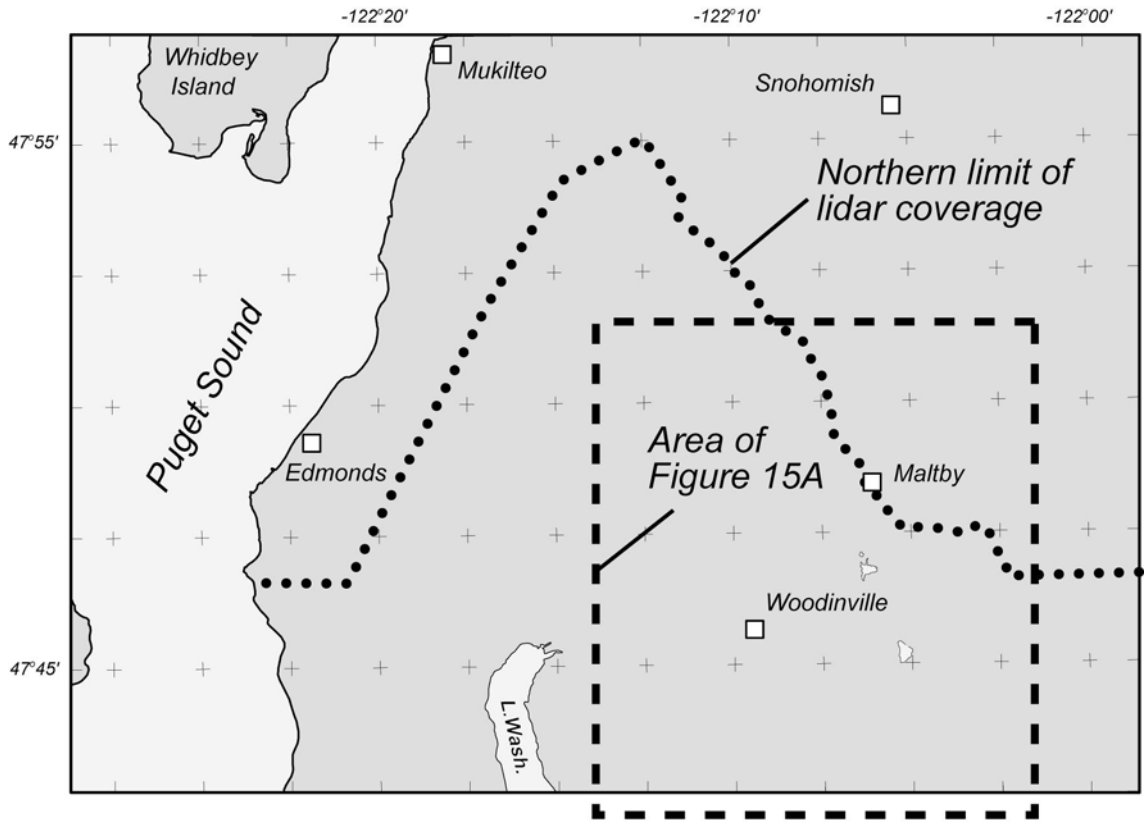

Figure 15B.-Map showing northern limit of lidar coverage and area of Figure 15A.

Figure 16.-Detailed lidar image showing locations of lineaments 1 through 3. White arrows point towards ends of the lineaments. Numbers refer to features discussed in text and shown in Table 3.

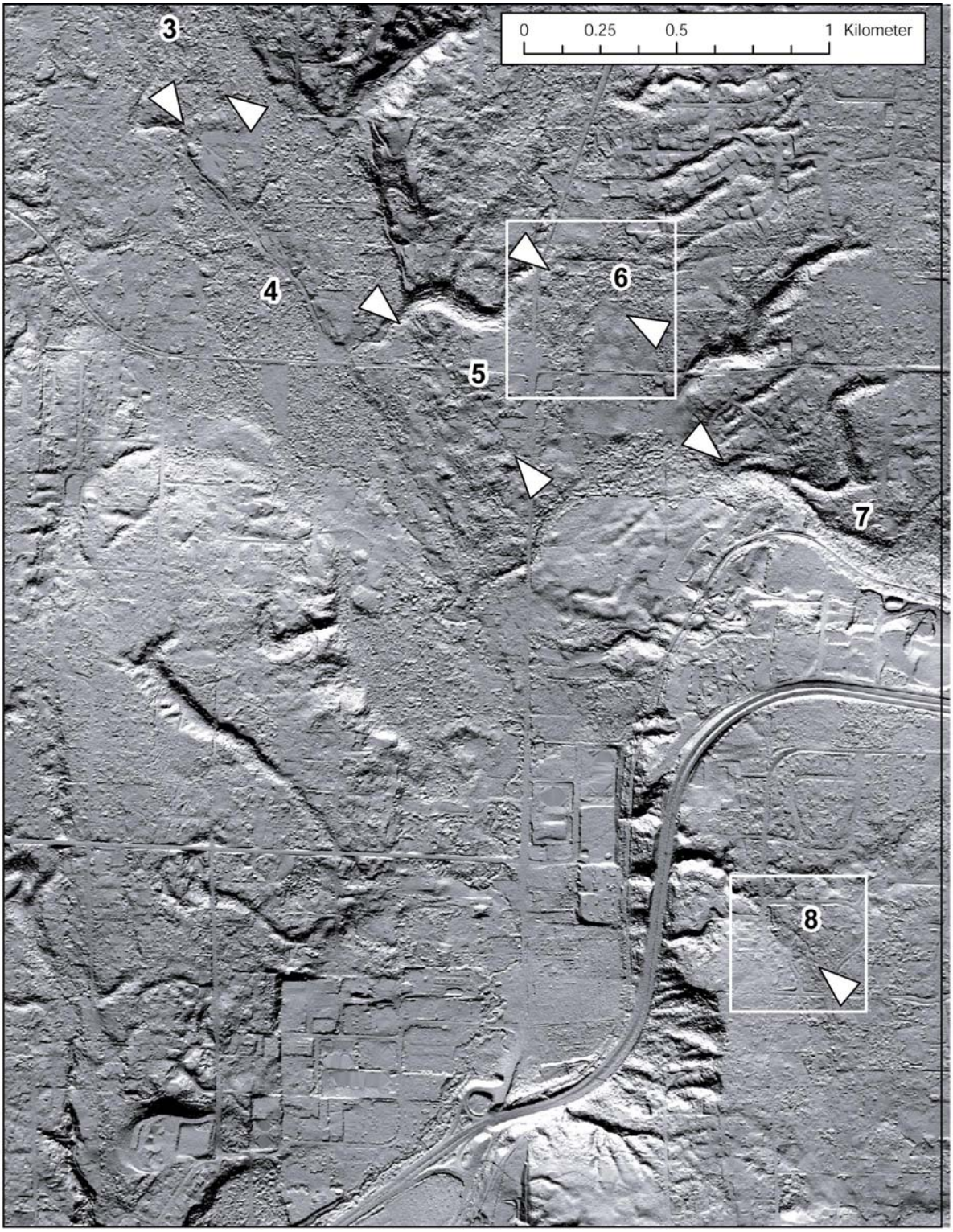

Figure 17.-Detailed lidar image showing locations of features 4, 5, 6 and 8. White arrows point towards ends of the lineaments. Numbers refer to features discussed in text and shown in Table 3. White boxes show locations of smaller-scaled lidar images in separate figures.

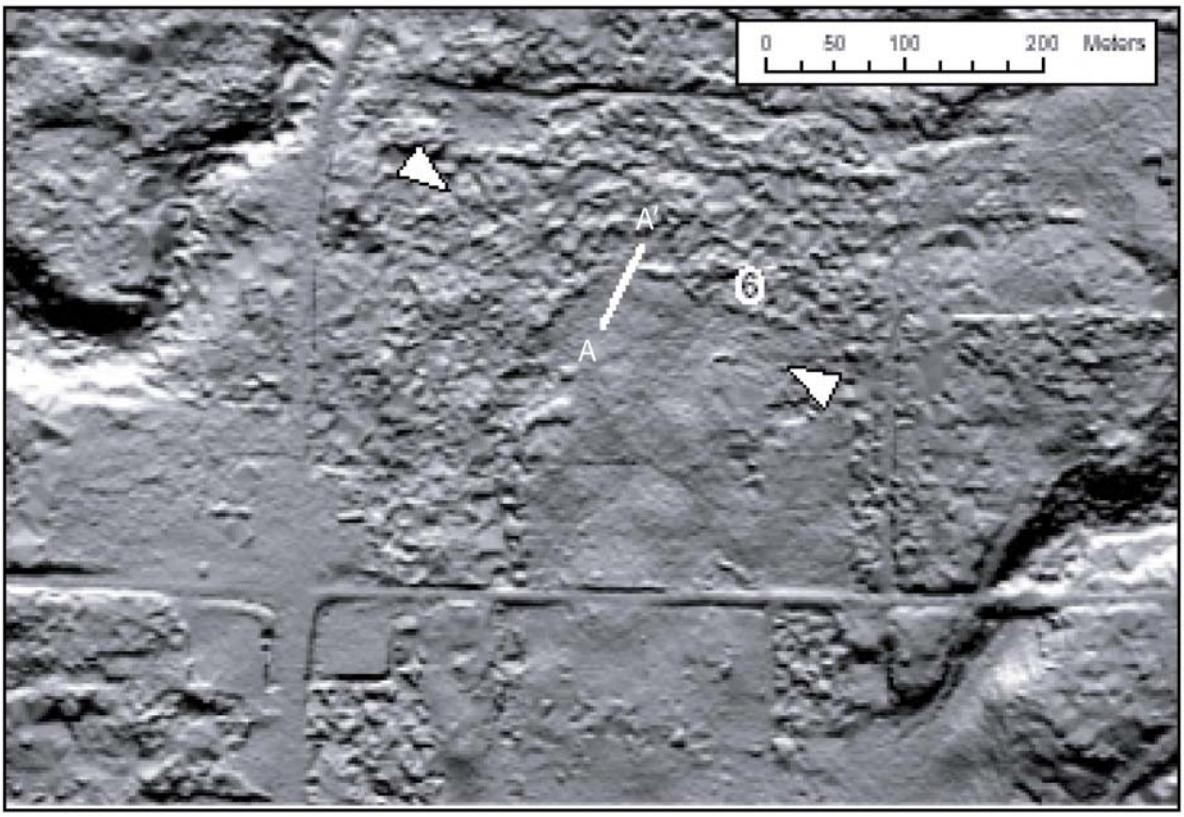

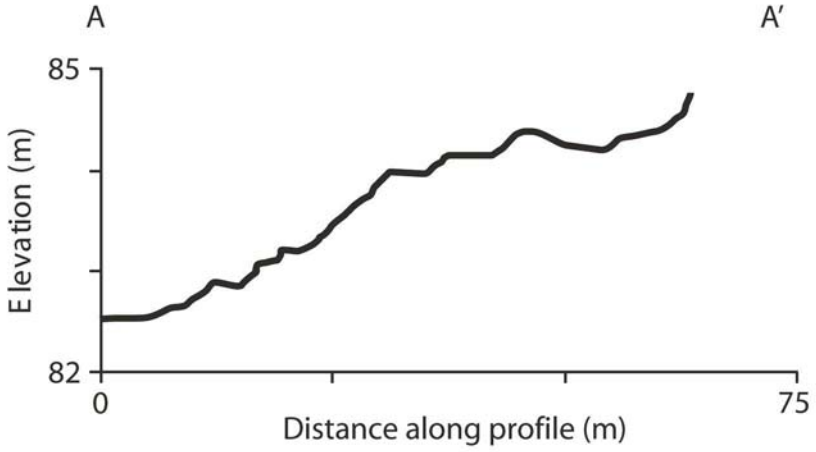

Figure 18.-Detailed lidar image showing locations of feature 6. White arrows point towards ends of the scarp. The location of profile A-A' is shown on the lidar image by a white line.

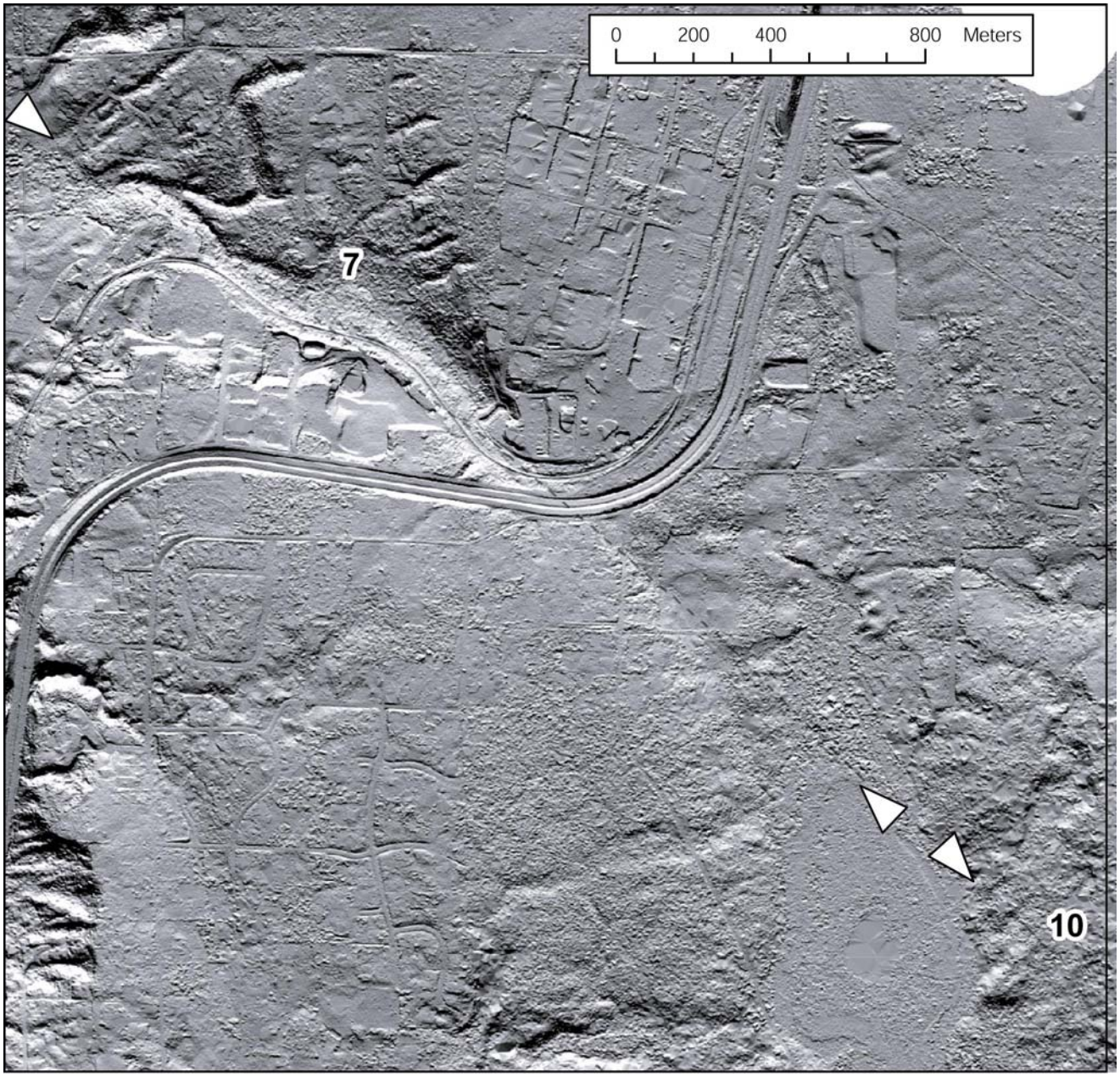

Figure 19.-Detailed lidar image showing location of lineament 7. White arrows point towards ends of lineament. Numbers refer to features discussed in text and shown in Table 3.

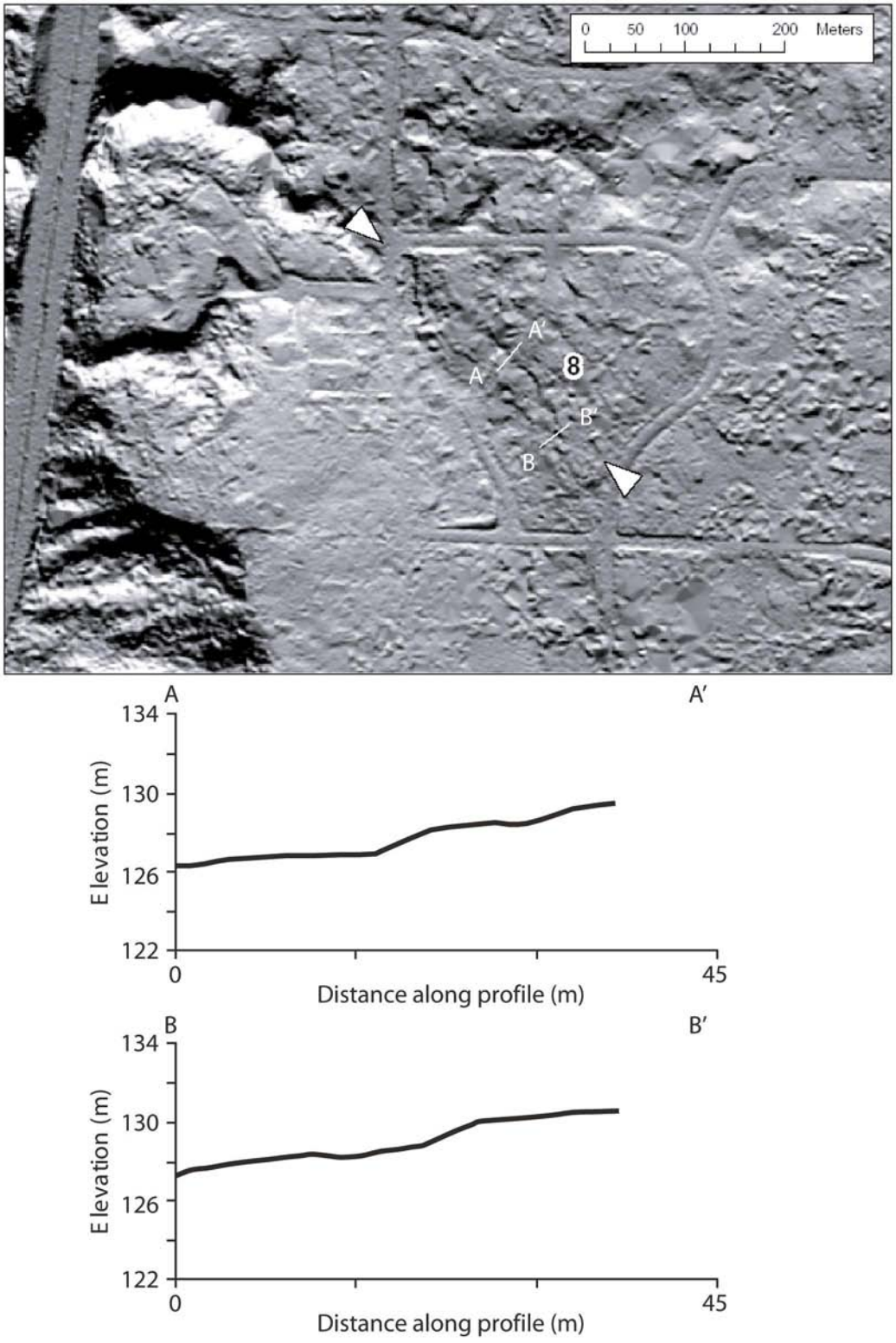

Figure 20.-Detailed lidar image showing locations of feature 8. White arrows point towards ends of the scarp. The location of profile A-A' and B-B' are shown on the lidar image by white lines.

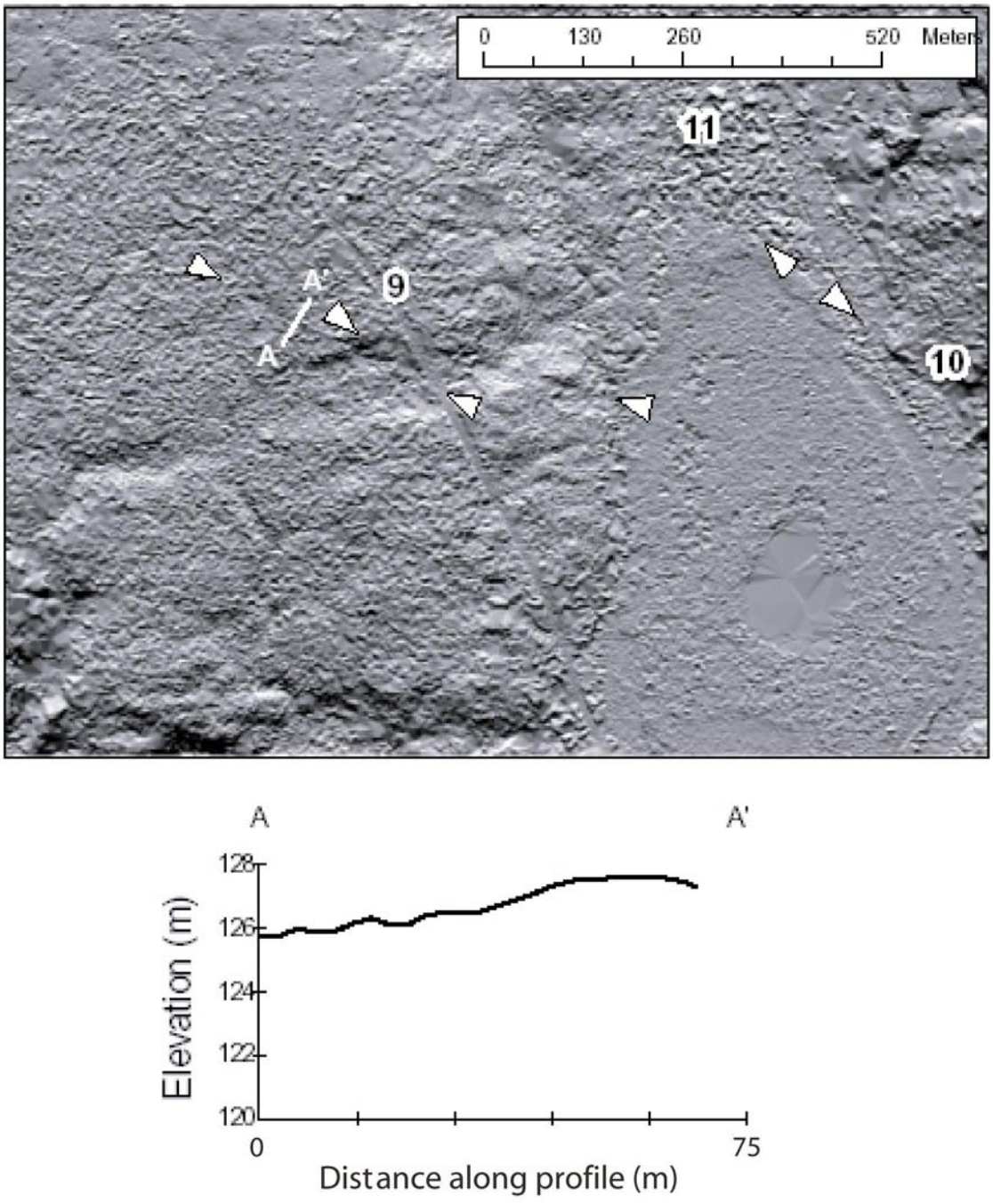

Figure 21.-Detailed lidar image showing locations of feature 9. White arrows point towards ends of the scarp. The location of profile A-A' is shown on the lidar image by a white line.

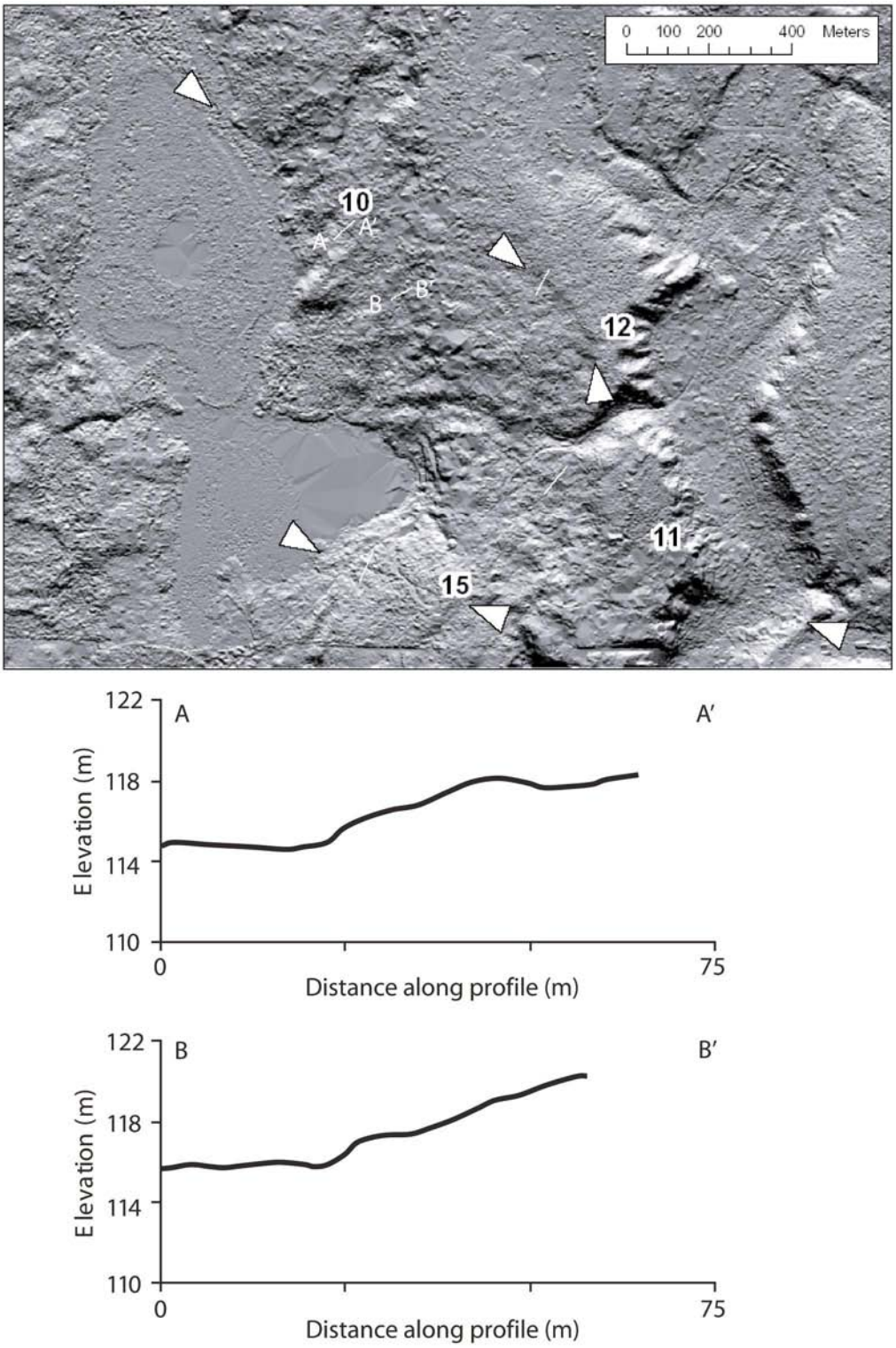

Figure 22.-Detailed lidar image showing locations of feature 10. White arrows point towards ends of the scarp. A-A' and B-B' show location of two profiles across the scarp, bottom of figure.

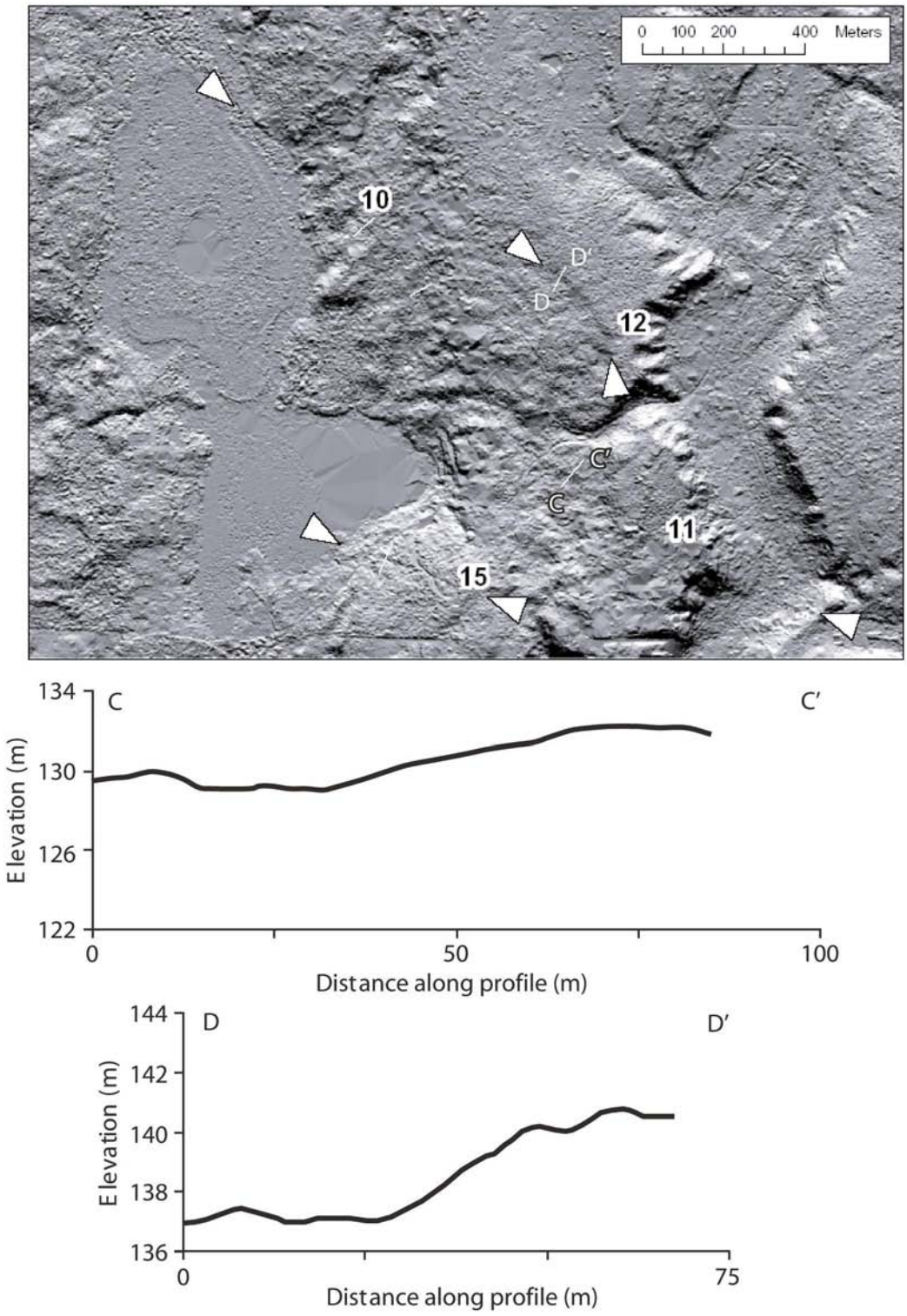

Figure 23.-Detailed lidar image showing locations of feature 11 and 12. White arrows point towards ends of the scarps. A profile across each scarp is shown in the plots below the lidar image. The locations of profile C-C' across feature 11 and profile D-d' across feature 12 are shown on the lidar image by white lines.

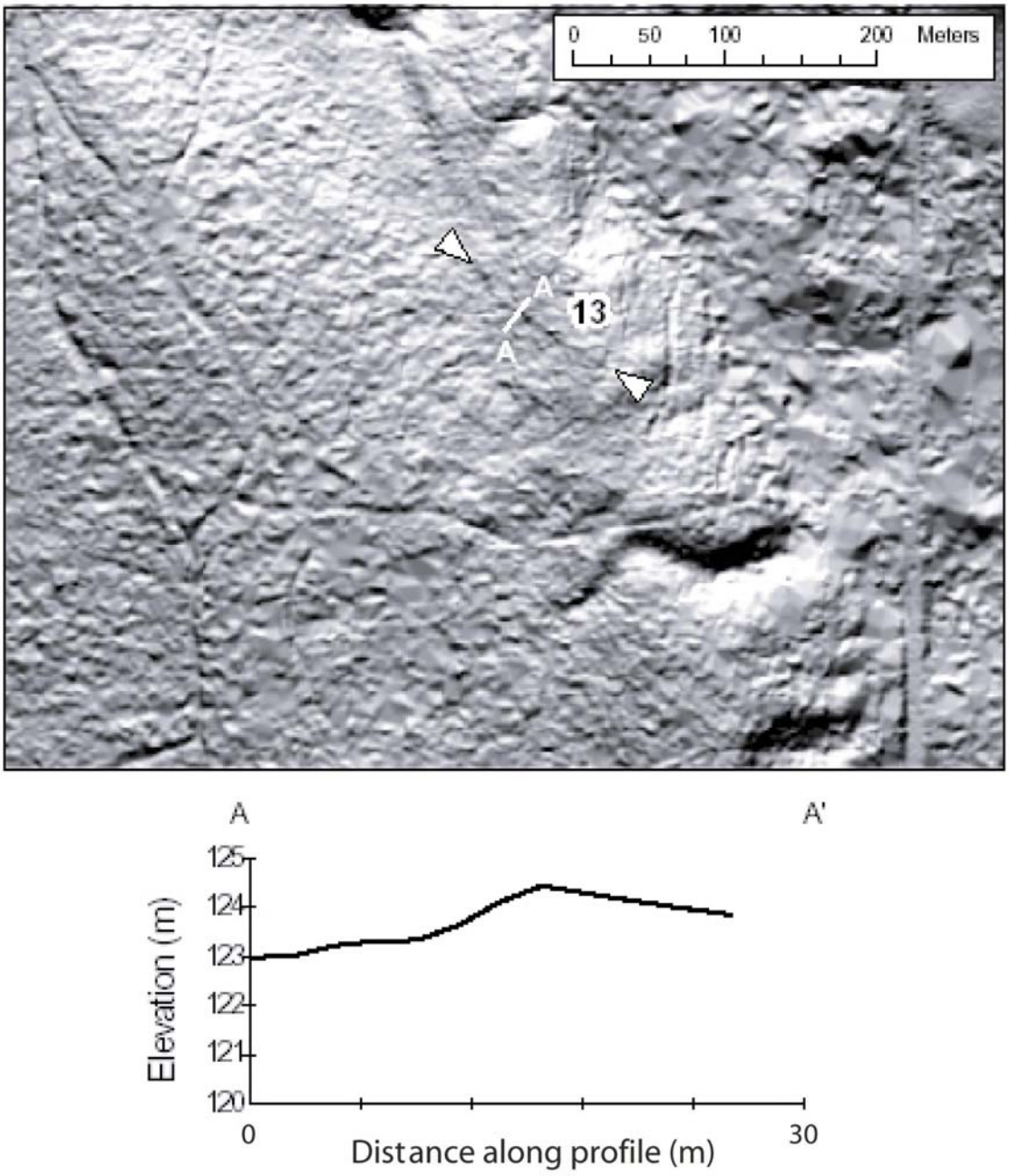

Figure 24.-Detailed lidar image showing locations of feature 13. White arrows point towards ends of the lineament. A profile across the scarp is shown in the plot below the lidar image. The location of profile A-A' is shown on the lidar image by a white line.

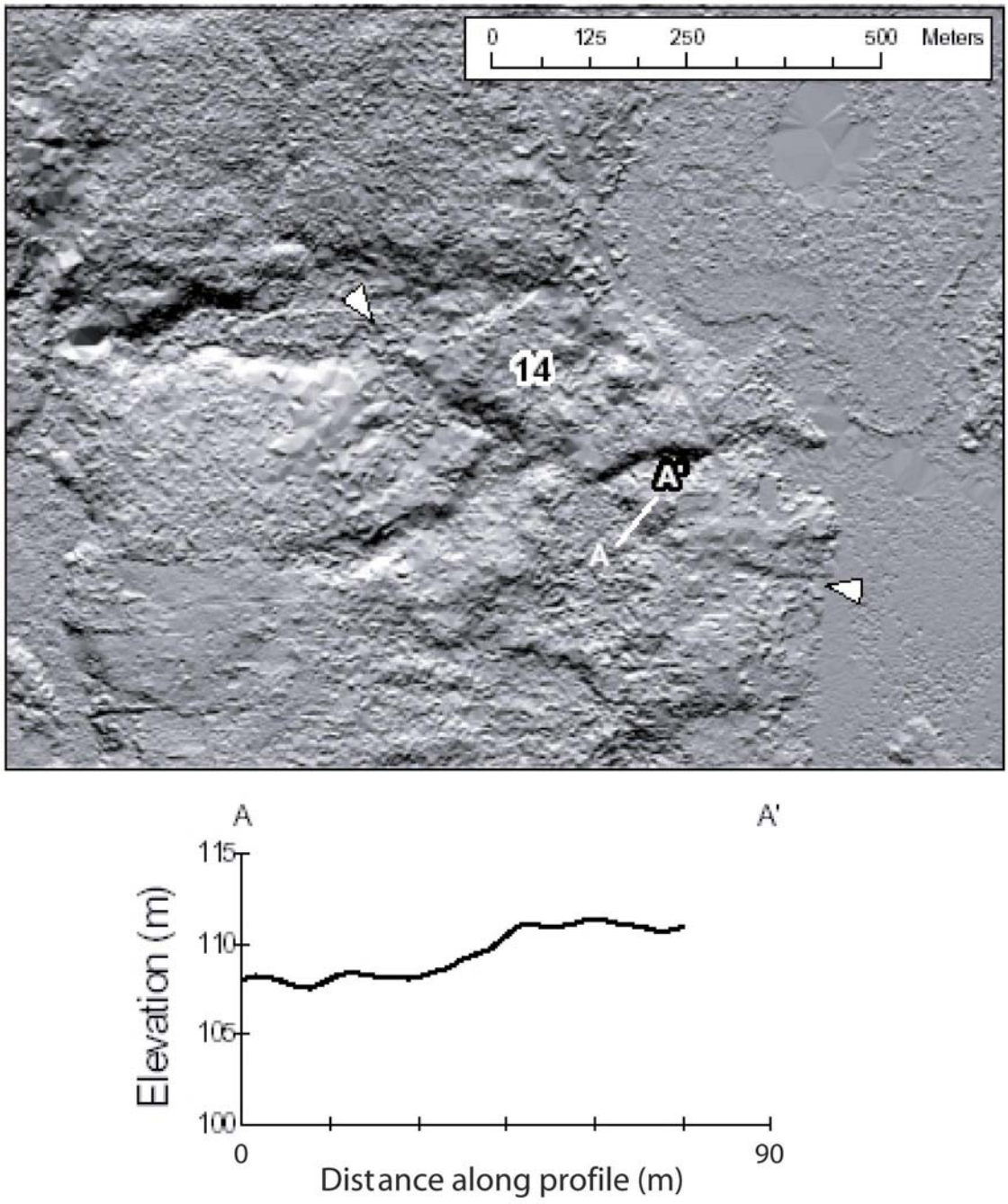

Figure 25.-Detailed lidar image showing locations of feature 14. White arrows point towards ends of the lineament. A profile across the scarp is shown in the plot below the lidar image. The location of profile A-A' is shown on the lidar image by a white line.

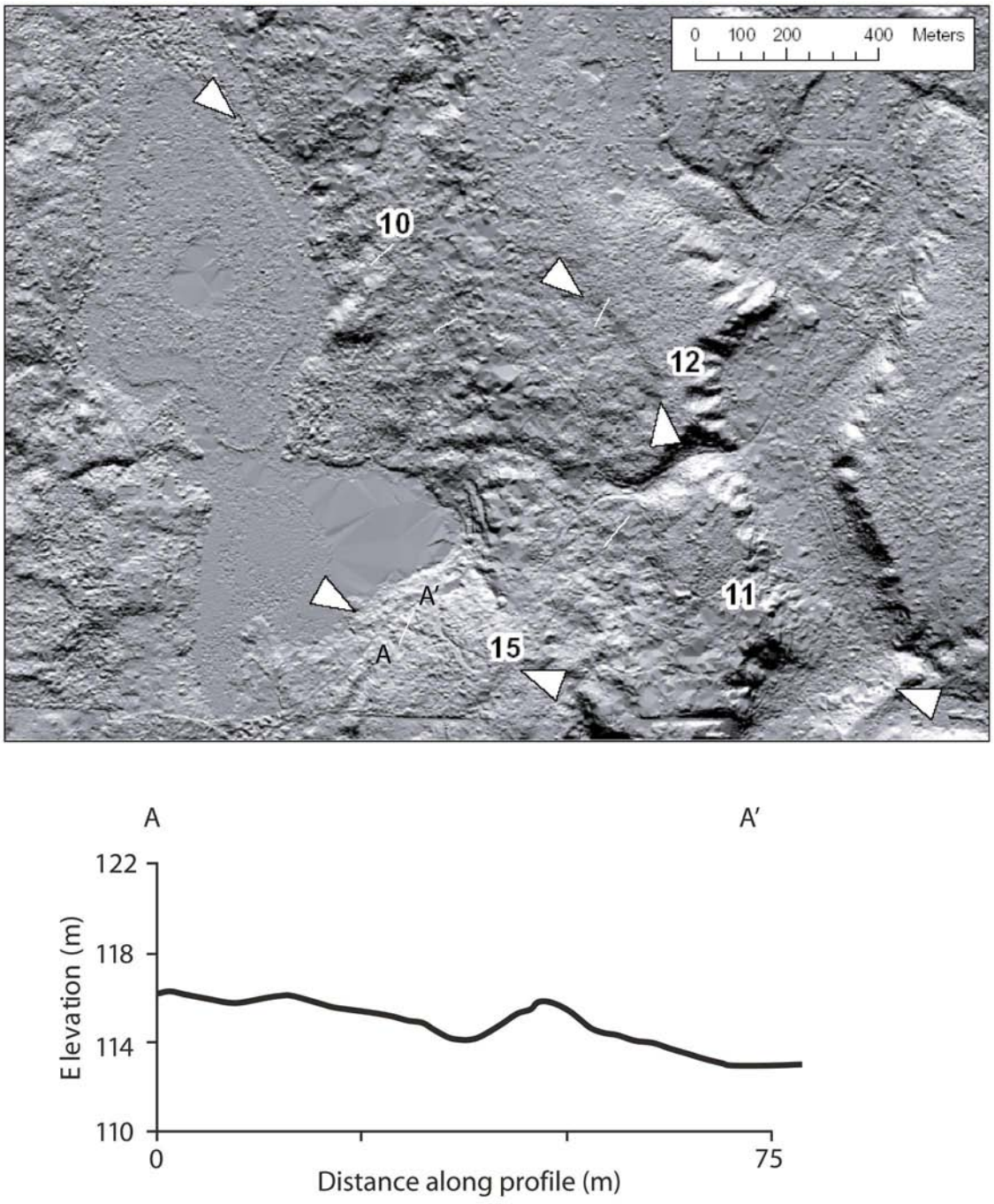

Figure 26.-Detailed lidar image showing locations of scarp 15. White arrows point towards ends of the lineament. A profile across the scarp is shown in the plot below the lidar image. The location of profile A-A' is shown on the lidar image by a white line.

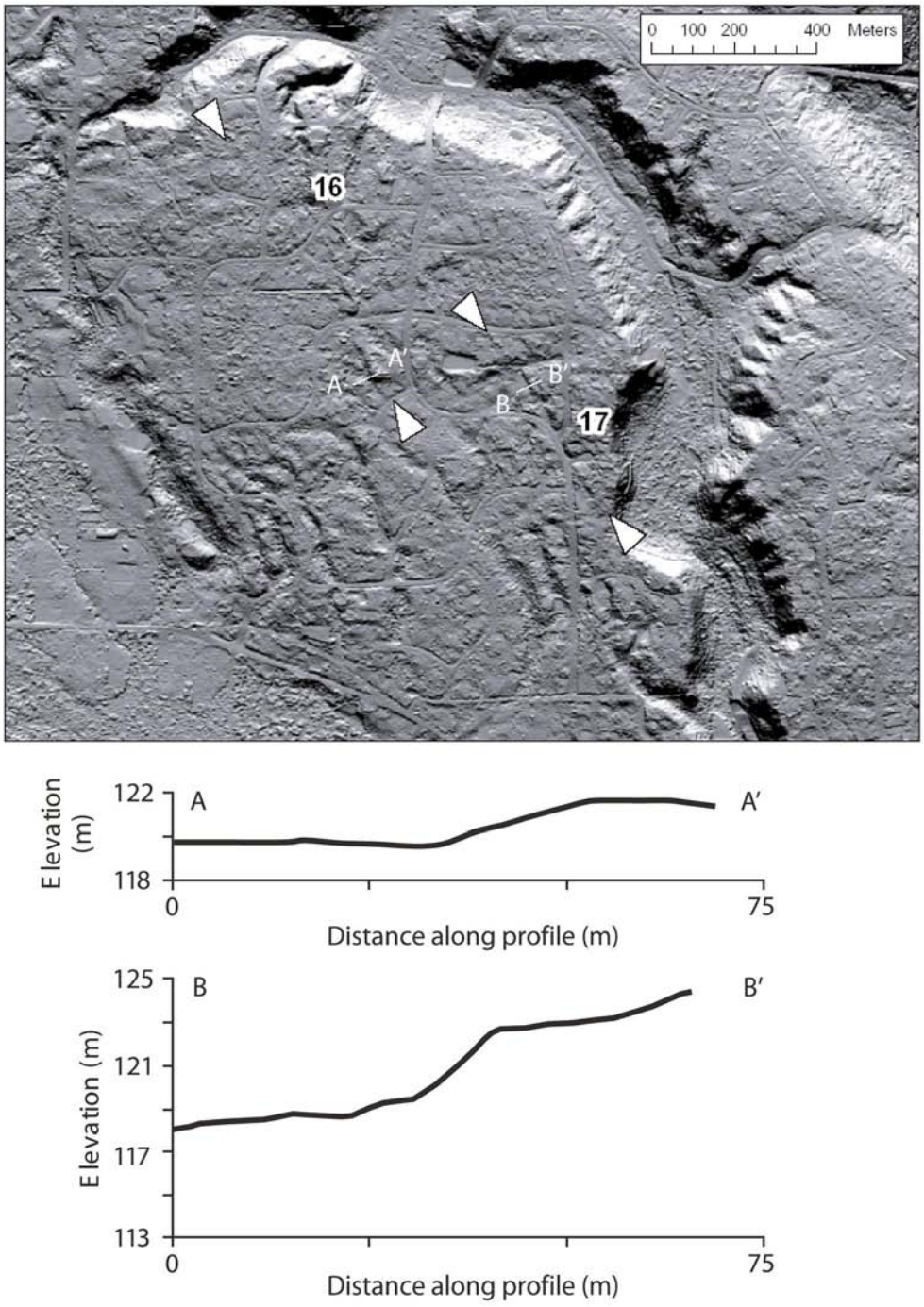

Figure 27.-Detailed lidar image showing locations of scarps 16 and 17. White arrows point towards ends of the scarps. A profile across each scarp is shown in the plots below the lidar image. The locations of profile A-A' across feature 16 and profile B-B' across feature 17 are shown on the lidar image by white lines.

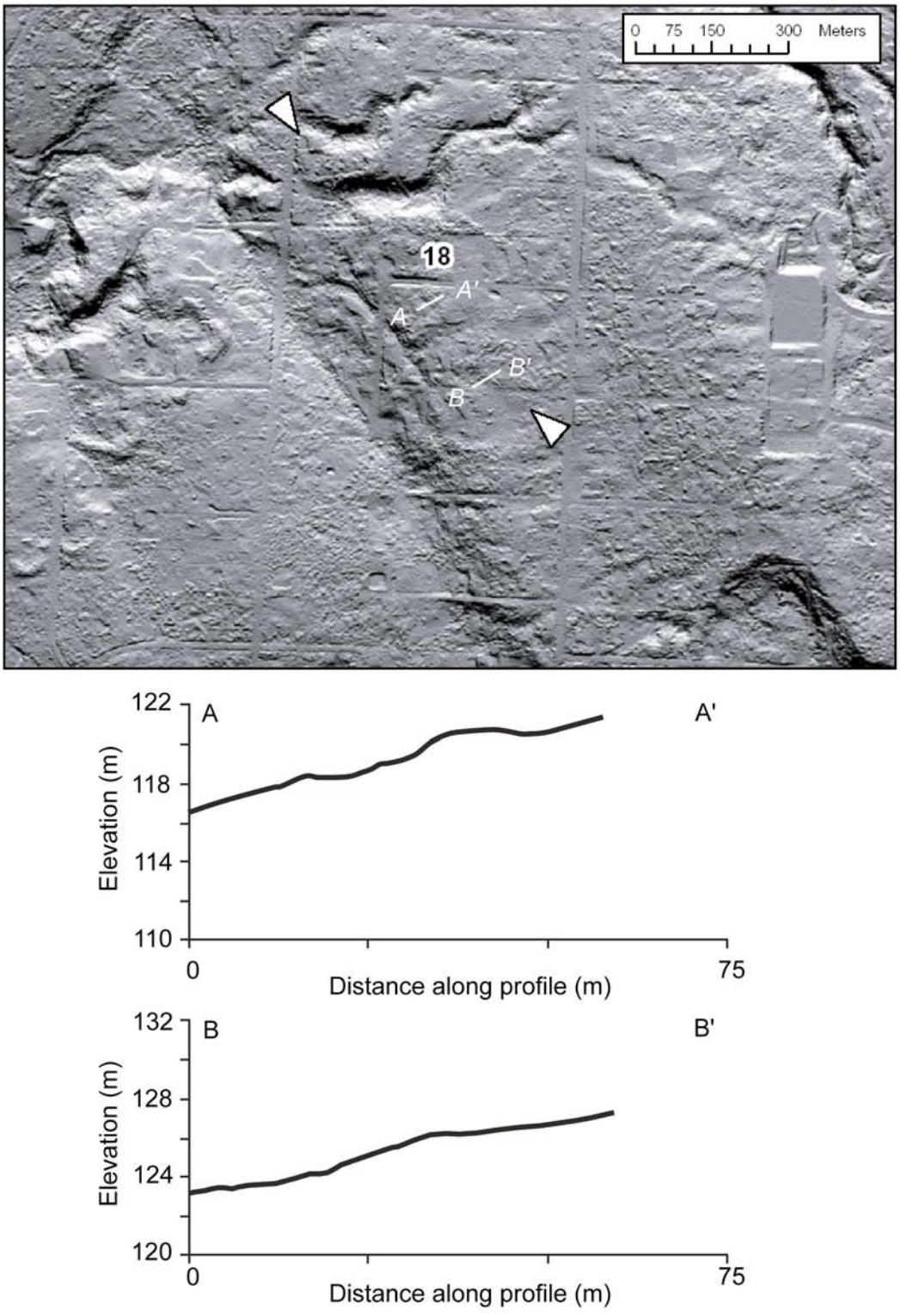

Figure 28.-Detailed lidar image showing locations of scarp 18. White arrows point towards ends of the scarps. Profiles across the scarp are shown in the plots below the lidar image. The locations of profile A-A' and profile B-B' are shown on the lidar image by white lines.

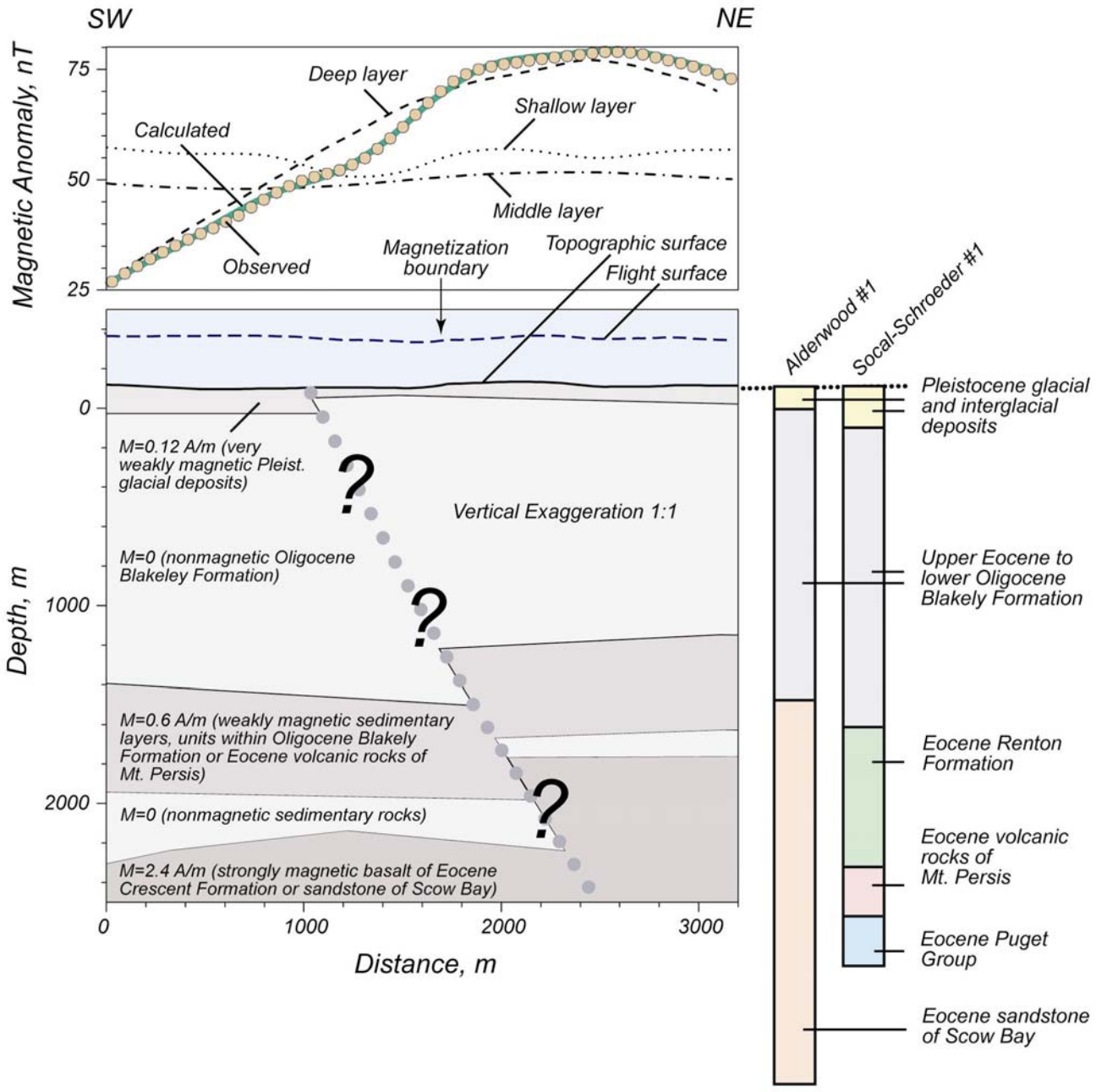

Figure 29.-Possible model for the Cottage Lake aeromagnetic lineament. See Figure 14 for location of profile. Model includes three magnetic units, from top to bottom: very weakly magnetic Pleistocene glacial deposits; a sequence of weakly magnetic sedimentary layers, possibly tuffaceous units within Oligocene Blakeley Formation or Eocene volcanic rocks of Mount Persis; basalts of the Eocene Crescent Formation or Eocene sandstone of Scow Bay. Stratigraphy of Alderwood #1 and Socal-Schroeder #1 wells from (Rau and Johnson, 1999). Bodies assumed infinitely extended perpendicular to profile. Remanent magnetization assumed negligible.